TECHNICAL REPORT 4806

THE MEASUREMENT OF AERODYNAMIC FORCES ON A SHORT BODY AT HIGH ANGLES OF ATTACK WITH THE MAGNETIC BALANCE SYSTEM

R. L. BISPLINGHOFF
J. B. COFFIN
E. E. COVERT
D. M. FINN
C. W. HALDEMAN

MASSACHUSETTS INSTITUTE OF TECHNOLOGY
AEROPHYSICS LABORATORY
CAMBRIDGE, MASSACHUSETTS 02139

DECEMBER 1974

PICATINNY ARSENAL
DOVER, NEW JERSEY

The findings in this report are not to be construed as an official Department of the Army Position.

DISPOSITION

Destroy this report when no longer needed. Do not return it to the originator.

Unclassified

SECURITY CLASSIFICATION OF THIS PAGE *(When Data Entered)*

REPORT DOCUMENTATION PAGE

READ INSTRUCTIONS BEFORE COMPLETING FORM

1. REPORT NUMBER: Technical Report 4806	2. GOVT ACCESSION NO.
3. RECIPIENT'S CATALOG NUMBER	
4. TITLE *(and Subtitle)*: THE MEASUREMENT OF AERODYNAMIC FORCES ON A SHORT BODY AT HIGH ANGLES OF ATTACK WITH THE MAGNETIC BALANCE SYSTEM	5. TYPE OF REPORT & PERIOD COVERED: Final 3/13/74 - 12/31/74
	6. PERFORMING ORG. REPORT NUMBER: MIT TR 190
7. AUTHOR(s): R L Bisplinghoff, J B Coffin, E E Covert, D M Finn, C W Haldeman	8. CONTRACT OR GRANT NUMBER(s): DAAA21-74-C-0304
9. PERFORMING ORGANIZATION NAME AND ADDRESS: Massachusetts Institute of Technology, Aerophysics Laboratory, Cambridge, Massachusetts 02139	10. PROGRAM ELEMENT, PROJECT, TASK AREA & WORK UNIT NUMBERS: AMCMS 662617.11.87906
11. CONTROLLING OFFICE NAME AND ADDRESS: U.S. Army, Picatinny Arsenal, Dover, New Jersey	12. REPORT DATE: December, 1974
	13. NUMBER OF PAGES: 77
14. MONITORING AGENCY NAME & ADDRESS *(if different from Controlling Office)*	15. SECURITY CLASS. *(of this report)*: Unclassified
	15a. DECLASSIFICATION/DOWNGRADING SCHEDULE

16. DISTRIBUTION STATEMENT *(of this Report)*

Approved for Public Release; Distribution Unlimited.

17. DISTRIBUTION STATEMENT *(of the abstract entered in Block 20, if different from Report)*

18. SUPPLEMENTARY NOTES

19. KEY WORDS *(Continue on reverse side if necessary and identify by block number)*

Magnetic balance
S-curve body
Aerodynamic testing

20. ABSTRACT *(Continue on reverse side if necessary and identify by block number)*

Aerodynamic lift coefficient, drag coefficient and pitching moment coefficient are reported for a short finned body at angles of attack from -20 to +20 degrees as measured with the magnetic balance system at M=.18 and .37, Re_d=1x10^5 and 2x10^5. Also reported are modifications made to the magnetic balance system in order to extend the angle of attack range. A new controllable D.C. power supply was constructed using 300 ampere, 30 volt D.C. aircraft generators. The steady state and transient response

DD FORM 1 JAN 73 1473 EDITION OF 1 NOV 65 IS OBSOLETE Unclassified

SECURITY CLASSIFICATION OF THIS PAGE *(When Data Entered)*

20. characteristics of this power supply are reported.

TABLE OF CONTENTS

FOREWORD

This work was performed at the Aerophysics Laboratory, Massachusetts Institute of Technology, Cambridge, Massachusetts 02139. The work was sponsored by the U.S. Army Munitions Command, Picatinny Arsenal, Dover, New Jersey 07801 under Contract No. DAAA21-74-C-0304. The contract was monitored by Mr. Henry Hudgins, Aeroballistics Branch, Picatinny Arsenal, Dover, New Jersey. Overall supervision of this study was provided by Professor Eugene E. Covert of the M.I.T. Aerophysics Laboratory in the capacity of Principal Investigator. The report covers work performed during the period March 13, 1974 to December 31, 1974.

The authors would like to thank the NASA Langley Research Center for the use of the magnetic balance equipment.

ABSTRACT

Aerodynamic lift coefficient, drag coefficient and pitching moment coefficient are reported for a short finned body at angles of attack from -20 to +20 degrees as measured with the magnetic balance system at M = .18 and .37, Re_d = 1 x 10^5 and 2 x 10^5. Also reported are modifications made to the magnetic balance system in order to extend the angle of attack range. A new controllable D.C. power supply was constructed using 300 ampere, 30 volt D.C. aircraft generators. The steady state and transient response characteristics of this power supply are reported.

NOMENCLATURE

a,b,c	- cartesian coordinates referenced to model
x,y,z	- cartesian coordinates referenced to balance
A.C.	- alternating current
B	- magnetic field intensity
B_a	- average applied magnetic field intensity in a direction
B_b	- average applied magnetic field intensity in b direction
B_x	- average value of axial (magnetizing) field
B_{xx}	- average value of $\partial B_x/\partial x$ over model volume
B_y	- average value of transverse magnetic field (horizontal)
B_{xy}	- average value of $\partial B_x/\partial y$ over model volume
B_z	- average value of transverse magnetic field (vertical)
C_D	- drag coefficient = drag $\div$ q $\frac{\pi}{4} D^2$
C_L	- lift coefficient = lift $\div$ q $\frac{\pi}{4} D^2$
C_M	- pitching moment coefficient referenced to diameter
D	- model diameter
D_a	- average demagnetizing factor in a direction (longest dimension)
D_b	- average demagnetizing factor in b direction
D_c	- average demagnetizing factor in c direction
D_x	- average demagnetizing factor in x direction
D.C.	- direct current

NOMENCLATURE (continued)

E_a - armature voltage

E_f - field voltage

F_x - force x direction

F_y - force y direction

I_f - field current

I_x - magnetization current

I_z - current in transverse field (B_z) coil

K_t - magnetic moment constant

KVA - kilovolt amperes

L - model length

M - Mach number, pitching moment

P - pressure

q - tunnel dynamic pressure

Re_d - Reynolds number referenced to diameter

γ_{pm} - revolutions per minute

T_b - torque

V - volume

α - pitch angle

α_s - pitch angle = $\tan^{-1}(\frac{B_Z}{B_X}) - \alpha$

LIST OF TABLES AND FIGURES

LIST OF TABLES AND FIGURES (continued)

INTRODUCTION

For many years magnetic suspension systems for wind tunnel models have been in use at the M.I.T. Aerophysics Laboratory. The study of the original balance system included design of a new power supply for the pitch and yaw degrees of freedom which would permit operation at higher angles of attack. Until recently this phase of the original design was not implemented. Under PA Contract No. DAAA21-74-C-0304 the original design study was reviewed as was the balance capability to support models in the range of $\pm 20^{\circ}$ angle of attack up to a velocity of 400 feet per second. As a consequence, a power supply was designed and a prototype tested. This power supply was then built and data was obtained at angles of attack from -20 to +20 degrees. This report describes the original balance limits, the choice of surplus aircraft generators for the power supply, the model design used, and the data obtained for the short blunt, finned body configuration. Care was taken to ensure that the new power supplies were compatible with the existing configuration, which has allowed recording accurate Magnus force data (References 1-3).

DISCUSSION

(a) LIMITATIONS OF THE NASA PROTOTYPE MAGNETIC BALANCE SYSTEM

As part of the research program the power limits of the present balance connection were determined. Possible alternatives for extending these limits will be discussed in the next section. The cooling limits of the coils, the actual power circuit connection for each degree of freedom, and the original power supply limits are discussed here.

Cooling Limits

Based on an assumed 140°F temperature rise, the measured water flow rate at 40 psi, and the resistance measured or calculated for the longest turn, the maximum current versus water pressure was calculated for each type of coil. Differences among coils of a given type were sufficiently small that they do not affect the results which are plotted in Figure 1. Flow rates at pressures above 40 psi were extrapolated assuming water mass flow varies as $\sqrt{\Delta P}$. This is a compromise fit between the pressure drop for a straight pipe and the pressure drop for a coil with large secondary flow effects (Reference 4). The total water demand per circuit is shown in Figure 2.

From Figure 1 it can be seen that the drag, magnetizing and outer saddle coils have the lowest limits; however, at the present time there is sufficient power available to require more than 40 psi cooling pressure only in the magnetizing coils. For other coils, 40 psi should provide adequate cooling up to 224 amperes in drag, 240 amperes in the outer saddles, 340 amperes in the inner saddles, and 380 amperes in lift and side force. As these current levels are above the levels achievable with the new power supply, the cooling limit is not a restriction at the present or proposed current levels.

Present Balance Circuitry

The present circuit connection of the NASA prototype balance uses a combination of adjustable uncontrolled bias from regulated magnetic amplifiers and controllable D.C. power from the original magnetic balance Thyratron power supplies. One of these supplies is a nominal 220 volt, 100 amp unit; two are 110 volt, 100 amp units; and two are 110 volt, 50 amp units. All are one-sided; i.e., the

output varies from 0 to a positive voltage level. The 100 amp supplies are presently connected to power lift, pitch and yaw with the small supplies connected to drag and side force.

The circuits consist of the coils, isolating resistors, ripple filters, roll power and EPS signal isolators (Figures 7 and 8, pitch and yaw only), metering shunts and the bias and control power supplies. The circuits with pertinent circuit constants are given in Figures 3-8. All coils are wound with .195" square copper conductors with a .130" diameter cooling hole.

(b) DESIGN OF NEW POWER SUPPLY FOR PITCH AND YAW

Calculation of model support capability for the balance indicated that increased power was needed in the pitch and yaw degrees of freedom to increase angles of attack above 10^{o}. A motor generator supply utilizing three 300 amp, 30 volt Government surplus aircraft generators was constructed, tested and used to operate the balance. This section presents the data that was obtained in order to make a choice among available generators.

During original design and construction of the NASA prototype magnetic balance, various power supply types were investigated as possibilities for the balance system. At that time motor generators with rapid field control were recommended. This type of supply had the following advantages:

1) It was double sided, thus a 40 KVA machine could provide full power at plus or minus polarity with a smooth transition across zero.

2) It could both give and absorb power under transient conditions in excess of its continuous rating by using inertial energy storage, thus when reversing the field in a coil the stored energy would not be lost as it would with a rectifier supply.

3) Overdrive of the field on a transient basis could improve the time response without exceeding D.C. current limits.

4) Commutator ripple would be much lower in amplitude and higher in frequency than rectification ripple. Filtering, if required at all, would thus be simpler.

The anticipated disadvantages were:

1) Difficulty was anticipated in obtaining machines with fast enough time response

2) Weight was large and hence, capital cost would be high

The first part of this section describes the results of tests of three types of Government surplus aircraft generators and a Lincoln welding machine to determine their performance as balance power supplies. The second part describes the measured performance of the final power supply. The machines tested are listed below:

Machines Tested

Generator	Manufacturer	Type and Number
1) Aircraft starter generator used on filament supply	Lear Siegler	Mod 230-64-002 Spec 204-060-200
2) Aircraft generator	General Electric	Type(R-1) 2CM73B6
3) Aircraft generator	Westinghouse	A-45-J-244
4) Welding machine	Lincoln	SAE 300
5) Aircraft generator	General Electric	2CM73B7

On all machines tested the loaded armature time response was close to that of the field when excited independently. Also, on all machines the measured time response at full excitation was shorter by more than a factor of two compared to the small signal time response.

A summary of the test results is given in Table 1.

Table 1

SUMMARY OF GENERATOR CHARACTERISTICS

Generator	Current Rating Amperes	Field Excitation Volts	Time Constant[1] Milliseconds	Linear Gain[2] Constants	Figure for Data
1	300	5	142	3.25	11
		10	110		
		20	55		
2	300	5	120	2.86	12
		10	100		
		15	55		
		20	60		
3	400	5	160	3.83	13
		10	133		
		20	100		
		25	73		
4	300	130	385	.85	
5	300	Essentially the same as 2 (Figure 12)			

(1) Measured from Polaroid photographs as the time to reach .632 x final amplitude.

(2) Armature volts per field volt at 3500 rpm. Generators 1, 2 and 3 can operate from 3000 to 10,000 rpm. Generator 4 is fixed at 3500.

Test Procedure

Since Generator 1 was the only machine already mounted with a motor, only this generator was operated under load (1/4 ohm) as well as with the armature open circuited. Generators 2 and 3 were operated at 2050 and 2000 rpm respectively using the Bridgeport milling machine to rotate the armature. For time response measurements, field voltage and armature voltage were displayed on a Tektronix 502 dual beam oscilloscope and Polaroid photographs of the response were made. Photographs were then used to obtain

values of $E_a/E_{a\ Final}$ versus time. These were plotted as $(E_{Final} - E)/E_{Final}$ versus time in Figures 9 and 10 for Generator 1.

Figure 9 indicates that the response of this generator is approximately exponential, as assumed, since the points fall close to a straight line. Note, however, the highly non-linear behavior as excitation is increased. This decrease in the time constant with increasing excitation would be expected since as the iron saturates, the field inductance decreases.

Since the armature inductance is expected to be very small, it is expected that the field time constant would control the generator response. Figure 10 shows this clearly for 10 volt field excitation.

Both E_a and I_f are approximately exponential with time and differences in the field and armature response time are not significant. This indicates that total time constant of the system could be markedly reduced by adding resistance in series with the field. While this would require additional power from the driver amplifiers, the total power required would be much less than that required with the present system of load resistors, which are in series with the balance coils. To check this experimentally, a 10 ohm resistor was inserted in series with the 2.4 ohm field of Generator 1, thus providing an excitation corresponding to 19.3 volts across the field. This reduced the armature output time response to 20 milliseconds and the field time response to 12 milliseconds (cf. Table 1).

D.C. Output Characteristics

D.C. output voltage of the machines tested is plotted as a function of field excitation in Figures 11-13. Because Generator 1 was already motor driven, it was tested both loaded and unloaded. Figure 11 shows that series field compounding in Generator 1 is effective in making the output independent of current until field saturation, where gain rapidly deteriorates. Characteristics of Generators 2 and 3 are shown in Figures 12 and 13. These are very similar to Figure 3. All exhibit a small residual field effect of about 1/2 volt at zero excitation. Otherwise, the response is symmetrical about zero. The Lincoln welder output, not plotted, indicates a linear range of about 80 volts. Because of its design with a high voltage field,

the gain is much lower than the other machines. Also, the welder time response of 385 ms. is quite long.

Commutator Noise

Polaroid photographs of the commutator ripple of Generator 1 with a 1/4 ohm resistive load were taken to determine the type of noise to be expected on the output signal.

Using dividers the following frequency components were identified on three photographs:

Component	Frequency Hertz	Amplitude Ratio Peak to Peak E_{DC}
f_0	1,250	.4%
f_1	2,500	1.4
f_2	12,500	.16%

The measured characteristics of Generator 2 were sufficiently encouraging that a power supply utilizing three generators, Type 2CM73B7, was constructed to power the inner and outer saddle coils. Because the field per volt applied to the outer saddle coil is about one-half that of the inner saddle coil because of the coil geometry, one generator was connected to the inner coils and two generators were connected in series to power the outer coils. The generator fields in each circuit were driven by a Torque System amplifier, No. PA-601, as shown in Figure 14.

The power supply, comprised of a 40 h.p. drive motor, cooling fan and three G.E. Model 2CM73B7 generators, was tested for both D.C. and A.C. response. The generators which were tested will be referred to as follows:

Generator	Serial Number
a	2205297
b	2200182
c	2205320

D.C. Measurements

For these tests the potential across the field terminals was controlled by a 10-turn 500 ohm potentiometer. The field and armature signals were displayed on a dual beam oscilloscope. For a prescribed field excitation the armature D.C. gain was noted and photographs were taken of the A.C. ripple. Figure 15 illustrates the gain curve for Generator c while Table 2 presents the comparative results for all three generators. It is noted that at most a 2-volt skewedness in the armature voltage exists over the positive and negative ranges of field excitation. A.C. ripple is presented in Table 3 for Generator c.

Table 2

COMPARISON OF GENERATOR ARMATURE OUTPUTS

E_{Field} (Volts D.C.)	$E_{Armature}$ (Volts)		
	Generator a	Generator b	Generator c
+2.5	+18	+20	+17
-2.5	-18	-18	-19
+5.0	+36	+38	+34
-5.0	-36	-36	-36
+10.0	+55	+56	+52
-10.0	-55	-54	-56
+20.0	* -	-	+64
-20.0	-	-	-65

*Power supply to E_{Field} insufficient to generate 20-volt potential. The output of a 6-volt battery was augmented by an amplifier with a gain of 28, thus allowing the extra data on Generator c.

Table 3

NO-LOAD ARMATURE RIPPLE (GENERATOR c)

E_{Field} (Volts D.C.)	A.C. Ripple (Peak-to-Peak Volts)
5.0	2.3
10.0	3.0
20.0	3.5

Frequency Response

Preliminary measurements were made to verify that the gain of the D.C. amplifier was constant for a frequency range of 10 to 100 cps with a sine wave generator. Since this gain was constant, the generator was tested without further regard for the amplifier's performance.

With the power supply in operation, a series of photographs were taken for field excitation voltages of 2.5, 5.0, 10.0 and 20.0 volts amplitude and a range of frequencies from 0.5 to 60 cps. The scope inputs A, B, C and D were connected to Points 3, 4, 5 and 6 respectively (Figure 16). Amplitude ratio and phase angle data were reduced from the Polaroid photographs taken of field and armature voltage under each test condition. Tables 4 and 5 present the frequency response data while Figures 17-22 illustrate the appropriate non-dimensionalized amplitude and phase angle curves.

Throughout the testing operation of the power supply appeared normal, without tendency to overheat or vibrate excessively. It will be noted in Figures 17-20 that the time constant of the system is specified by intersection of the asymptotes to the curve.

This time constant, while higher than might be desired for the most difficult models, has been found adequate for the S-curve bodies when incorporated into the complete closed loop control system. Use of this supply increased the operating angle of attack range by about a factor of 2 for the S-curve body model.

Improvements in other components of the system, notably the 5 mh chokes nearest the saddle coils in Figures 7 and 8, which are presently limiting pitch and yaw current, and the lift, drag and side force supplies, which limit these forces, would extend angle of attack range even more.

Table 4

AMPLITUDE RATIO FREQUENCY RESPONSE

	$E_{Arm}/(E_{Arm})_{D.C.}$			
ω(cps)	Amplitude E_f = 2.5v	Amplitude E_f = 5.0v	Amplitude E_f = 10.0v	Amplitude E_f = 20.0v
0.5	.861	.857	.944	.930
1.0	.722	.743	.870	.930
2.0	.472	.514	.648	.837
4.0	.278	.3	.389	.550
6.0	.2	.214	.278	.403
8.0	.15	.171	.222	.318
10.0	.117	.131	.176	.256
14.0	.089	.094	.130	.186
18.0	.072	.076	.102	.155
20.0	.064	.069	.093	.140
25.0	.053	.054	.073	.116
30.0	.044	.046	.063	.093
60.0	.02	.024	.030	.047

Table 5

PHASE ANGLE DATA

	Amplitude E_f = 2.5v			Amplitude E_f = 5.0v			Amplitude E_f = 10.0v			Amplitude E_f = 20.0v		
ω(cps)	X	Y	Φ	X	Y	Φ	X	Y	Φ	X	Y	Φ
0.5	2.2	.2	32.73	2.1	.1	17.14	2.15	.1	16.74	2.15	.1	16.74
1.0	1.1	.1	32.73	1.08	.12	40.00	1.12	.12	38.57	1.1	.11	36.00
2.0	.55	.1	65.45	.55	.08	52.36	.55	.08	52.36	.56	.06	38.57
4.0	.28	.05	64.29	.27	.05	66.67	.275	.05	65.45	.27	.05	66.67
6.0	.19	.04	75.79	.18	.035	70.00	.18	.035	70.00	.18	.03	60.00
8.0	.14	.025	64.29	.135	.03	80.00	.14	.032	82.29	.14	.032	82.29
10.0	.11	.02	65.45	.109	.024	79.27	.11	.025	81.82	.112	.024	77.14
14.0	.079	.017	77.47	.078	.018	83.08	.08	.018	81.00	.08	.018	81.00
18.0	.061	.013	76.72	.062	.014	81.29	.063	.014	80.00	.062	.014	81.29
20.0	.058	.012	74.48	.056	.013	83.57	.055	.012	78.55	.056	.012	77.14
25.0	.044	.0095	77.73	.045	.01	80.00	.045	.01	80.00	.045	.01	80.00
30.0	.038	.008	75.79	.037	.008	77.84	.036	.008	80.00	.037	.008	77.84
60.0	.018	.004	80.00	.018	.004	80.00	.018	.004	80.00	.018	.004	80.00

X = Period (sec)

Y = Phase Difference (sec)

$\Phi = 360^{o}$ (Y/X)

(c) MODEL DESIGN

Ellipsoidal Core Construction

The model geometry is shown in Figure 23. A brass exterior soldered to an ellipsoidal ingot iron core was machined to the dimensions shown, which were supplied by Picatinny Arsenal.

The ellipsoidal core was chosen because magnetic saturation (if it should occur in sharp areas of a model) could produce changes in magnetic balance calibration as the saturated volume changed due to combined magnetic field or model orientation changes.

Since a magnetic core in the shape of an ellipsoid of revolution would be uniformly magnetized, use of such a core would be expected to minimize such effects. Generalized ellipsoid coordinates were generated using

$$\frac{Y}{b} = \left(1 - \left(\frac{X}{a}\right)^2\right)^{1/2} \qquad (1)$$

the equation for an ellipse, where b is the semiminor axis, a is the semimajor axis, Y is the radial coordinate and X is the axial coordinate. These were then multiplied by a = 1.984, b = .5 to produce the ellipsoid coordinates given in Table 6.

Because of the need for a cylindrical region for chucking models and for use of the laser position sensor, the center section of the model core was made cylindrical by holding the center section of the ellipsoid to a .5 inch diameter cylinder. This core was then fitted into a model with L/D = 4.0. For the cylindrical region, the value of Y for a true ellipsoid is given in parentheses. Note that addition of a maximum of .004 inch provided a .472 inch wide cylindrical surface in the center of the model and provided a step of .004 in. radius to provide a stop in soldering. This shape was chosen as an acceptable compromise with a perfect ellipsoid which could not be mechanically handled easily.

Details of the assembled S-curve body model with the ellipsoidal core are given in Figure 23. Fins, nose and tail sections are made of brass soft soldered to the ingot iron core. This design proved satisfactory for the present non-spinning tests. Should a lighter non-conducting

Table 6

COORDINATES FOR ELLIPTICAL CORE:
L/D = 3.968; a = 1.984; b = .5

X (inches)	Y (inches)	Y*
0.	.500	(.500)
.01984	.500	(.49998)
.03968	.500	(.49990)
.05952	.500	(.49978)
.07936	.500	(.49960)
.09920	.500	(.49938)
.11904	.500	(.49910)
.13888	.500	(.49878)
.15872	.500	(.49840)
.17856	.500	(.49797)
.19840	.500	(.49749)
.21824	.500	(.49697)
.23808	.500	(.49639)
.25792	.49576	
.27776	.49508	
.29760	.49435	
.31744	.49356	
.33728	.49272	
.35712	.49184	
.37696	.49089	
.39680	.48990	
.41664	.48885	
.43648	.48775	
.45632	.48660	
.47616	.48539	
.4960	.48413	
.51584	.48281	
.53568	.48143	
.55552	.480	
.57536	.47952	
.59520	.47697	
.61504	.47537	
.63488	.47371	
.65472	.47199	
.67456	.47022	
.69440	.46838	

*For perfect ellipsoid.

Table 6 (continued)

X (inches)	Y (inches)
.71424	.46648
.73408	.46452
.75392	.46250
.77376	.46041
.79360	.45826
.81344	.45605
.83328	.45376
.85312	.45142
.87296	.4490
.89280	.44652
.91264	.44396
.93248	.44134
.95232	.43864
.97216	.43586
.9920	.43302
1.01184	.43009
1.03168	.42709
1.05152	.424
1.07136	.42084
1.09120	.41759
1.11104	.41425
1.13088	.41082
1.15072	.40731
1.17056	.40370
1.19040	.4
1.21024	.39620
1.23008	.39230
1.24992	.38830
1.26976	.38419
1.28960	.37997
1.30944	.37564
1.32928	.37118
1.34912	.36661
1.36896	.36191
1.3888	.35707
1.40864	.35210
1.42848	.34699
1.44832	.34173
1.46816	.33631
1.4880	.33072

Table 6 (continued)

X (inches)	Y (inches)
1.50784	.32496
1.52768	.31902
1.54752	.31289
1.56736	.30656
1.58720	.3
1.60704	.29322
1.62688	.28618
1.64672	.27888
1.66656	.27130
1.68640	.26339
1.70624	.25515
1.72608	.24653
1.74592	.23749
1.76576	.22798
1.78560	.21795
1.80544	.20731
1.82528	.19596
1.84512	.18378
1.86496	.17059
1.88480	.15613
1.90464	.14
1.92448	.12156
1.94432	.09950
1.96416	.07050
1.984	0.

material be required for future tests of this body in order to improve EPS response to a spinning model, the nose and tail sections can be made of G-10 fiberglass laminate. In this case, the core should probably be copper plated.

Estimate of Short Body Force Capabilities in Magnetic Balance using Ellipsoidal Core

Using the force and moment equations from Reference 5 and the circuit constants for the balance from Figures 3-8 and Reference 5, the force capabilities on an ellipsoid with L/D = 4 were estimated. The properties of this core were assumed to be L = 4", D = 1"

$$\text{Volume} = 2 \text{ in}^3$$

$$D_a = .075 \qquad D_b = D_c = .462$$

As an aid to model design D_a for ellipsoids is plotted in Figure 24 (from Reference 5).[a] Using this demagnetizing factor, the magnetizing field sensitivity $B_x = 19\ I_x$, and assuming the model is magnetized to 15,000 gauss, $M_x = 15{,}000 = B_x/D_x$ yields $B_x = 1120$ gauss, $I_x = 59$ amperes. Since the transverse field sensitivity $B_z = 3.5\ I_z$, the transverse field (pitch) current required to rotate the magnetization vector through a given pitch angle can be calculated. Values are given below as a function of α, the angle between the horizontal and $\bar{B}_x + \bar{B}_z$ vector. Note α is the angle of attack at zero pitching moment for a magnetically symmetric model.

Pitch Current Required to Achieve given α at $B_x = 1120$ gauss

α (degrees)	B_y (gauss)	I_z (amperes)	$\lvert B \rvert$ gauss
10	198	57	1137
20	409	117	1192
30	649	185	1294

Since the original limit of the pitch and yaw power supplies was ± 40 amperes, it is evident that pitch angles of 10 degrees could not be reached without additional power. It also indicates that the new pitch and yaw supply with about a ± 160 ampere capacity would make possible operation at about 26 degrees α. This is consistent with the measured performance since the 20^{o} limit in the tests was reached in lift.

The maximum aerodynamic q at which the balance would operate with this model can be estimated from the force equations and the model aerodynamic coefficients.

Approximate Force Equations

Neglecting the vector cross terms for model design,

$$F_x = K_T \, V \, M_x \, B_{xx} = \text{Drag Force} \qquad (2)$$

$$F_y = K_T \, V \, M_x \, B_{xy} = \text{Lift Force} \qquad (3)$$

Using K_T = 1.14 in lb/in^3 per kilogauss^2

$V = 2$ in^3

$B_{xx\ max}$ = 76 gauss/in; i.e. 45 amperes drag current

B_{xy} = 84 gauss/in; i.e. 60 amperes lift current

The maximum magnetic lift force is 2.9 lbs at 60 amperes.

The maximum magnetic drag force is 2.6 lbs at 45 amperes.

Approximate Torque Equations

Let the body angle of attack = α.

Then $\tan^{-1} \left(\frac{B_z}{B_x}\right)$ = angle of attack of magnetization field $\overline{B}_z + \overline{B}_x$

α_s = slip angle between model magnetic axis and magnetizing field vector.

Then the geometric model angle of attack α = $\tan^{-1}\left(\frac{B_z}{B_x}\right) \pm \alpha_s$. The pitching torque (from Reference 5)

$$T_b = K_T \, V \, B_a \, B_c \left(\frac{1}{D_c} - \frac{1}{D_a}\right) \qquad (4)$$

If α_s is sufficiently small and D_c/D_a is sufficiently large that $M_c/M_a \ll 1$,

$$T_b = K_T \, V \, B_a^{\,2} \tan \alpha_s \left(\frac{1}{D_c} - \frac{1}{D_a}\right) = -2.75 \tan \alpha_s \text{ in lbs}$$

If $\alpha_{s\,max} = 20^{\circ}$, $T_{b\,max} = 1.0$ in. lbs

Aerodynamic Forces

Using the aerodynamic coefficients for the configuration in Appendix A at q = 2 psi, the lift drag and pitching moment are listed below.

Lift, Drag and Pitching Moment
for S-Curve Body 1 inch in Diameter
and 4 inches long

α Body (degrees)	Lift (lbs)	Drag (lbs)	M about 1.72 calibers (in-lbs)	M about 2.0 calibers in-lbs
0	0	.156	0	0
4	-	-	.14	.24
10	.99	.452	0	.30
20	2.31	1.25	-.68	.06
30	4.23	2.71	-1.90	-.61

Use of the new power supply has closely matched this predicted performance. The full capacity of the new supply has not yet been used because the 5 mh chokes in the saddle coil circuit are operable only at 50 to 100 amperes. This

has not limited the present operating range because of the limits in lift.

(d) AERODYNAMIC DATA

Lift, drag and pitching moment data were recorded and reduced to coefficient form based upon the maximum diameter for areas and the reference length. Moments are referenced about an on-axis point 2 calibers from the nose. The data is presented graphically in Figures 25-30 and is tabulated in Appendix B. The data was recorded at Mach number of 0.18 and 0.37, corresponding to Reynolds numbers of about 100,000 and 200,000. The data is internally consistent and the accuracy is consistent with standard practice for M = .37. Scatter of the M = .18 pitching moment data is higher than normal because of the calibration method required. This scatter became excessive below -10 degrees. Since this represents the first data taken with the magnetic balance system at angles of attack of 10 degrees and higher, there is no "standard practice" yet established for high angles of attack. The lack of symmetry of the drag curve, Figure 29, at high positive and negative angles indicates a need for further work to identify if this is systematic error that can be eliminated by modifying the present experimental techniques.

Comparison with other data supplied by Picatinny Arsenal (Appendix A) shows a general lack of agreement. However, in view of the differences in Reynolds number and Mach number between the two tests, the differences are not unexpected. It is not known if an artificially tripped boundary layer would provide better agreement in view of the degree of bluntness of the model.

Calibration

Dead weight calibration of the model was performed at $0^{o} \pm 5^{o} \pm 10^{o} \pm 15^{o}$ and $\pm 20^{o}$. At 15^{o} and 20^{o} the load range was limited by the lift and drag power supplies. Because of this limitation only certain combinations of angle of attack, lift load and drag load could be used without overloading in either drag or lift. Specifically the model could not be held wind off at high positive angles of attack. For this reason wind off tares could not be taken immediately after each run by shutting down the wind tunnel drive motor with the model suspended. Wind off tares were, therefore, taken all at one time during calibration. This procedure necessarily led to larger uncertainty in the tare readings. Thus, at low speed with small q, the uncertainty in the sensitive moment data is larger than normal.

CONCLUSIONS

As a result of the above research the following conclusions can be drawn:

1. With the higher current available from the new power supply, data could be acquired from -20^{o} to $+20^{o}$ at M = .18 for a model having L/D = 4. Lack of power in other degrees of freedom is now the factor limiting the useful range of angle of attack and dynamic pressure.

2. The large difference in drag coefficient (Figure 26) between the present data and Reference 6 for the body tested is believed to be a result of the large difference in Reynolds number. This indicates that the performance of this shape in field applications will also be similarly Reynolds number dependent.

3. Power supplies using some types of surplus aircraft generators can be used successfully with at least some model configurations in the magnetic balance system.

4. Asymmetry in some magnetic balance force data which occurs between high negative and high positive angles of attack (see Figure 29) was observed in this test. Further research is indicated to identify its source and recommend experimental procedures for eliminating it.

REFERENCES

1. Coffin, J. B. and C. W. Haldeman, "Design and Initial Operation of a 3-Degree of Freedom Magnus Rotor in a Magnetic Balance System", Picatinny Arsenal TM 2069, January, 1973.

2. Haldeman, C. W., J. B. Coffin, E. P. Birtwell and M. Vlajinac, "Improvements in the Magnetic Balance System Required for Magnus Testing", Presented at the Fifth International Congress on Instrumentation in Aerospace Simulation Facilities, Pasadena, California, September 10-12, 1973.

3. Haldeman, C. W., J. B. Coffin, E. P. Birtwell and M. Vlajinac, "Magnus Measurements with the Magnetic Balance System", DAAD05-72-C-0181, MIT Aerophysics Laboratory TR 187, December, 1973.

4. Haldeman, C. W., "ARL Outer Saddle Coil Cooling", MIT Aerophysics Laboratory Internal Memorandum, April 20, 1967.

5. Stephens, T., "Design, Construction and Evaluation of a Magnetic Suspension and Balance System for Wind Tunnels", NAS1-4421, MIT Aerophysics Laboratory TR 136, November, 1969.

6. Brunk, J. E., "Monte Carlo Analysis of S-Curve and Roll through Zero Bomblet Dispersion Characteristics", Alpha Research Corporation Report, AFATL TR 73-15, January, 1973, p 19.

A P P E N D I C E S

APPENDIX A

AERODYNAMIC COEFFICIENT SUMMARY FOR BASIC S-CURVE CONFIGURATION $B_S N_{S1} A_{S2} F_{S3}$

AEROBALLISTIC COEFFICIENTS														
Coefficient	Mach Number	Angle of Attack - Degrees												
		0	2	4	6	8	10	12	16	20	24	30	60	90
CX	0-0.5	-.100	-.103	-.128	-.154	-.169	-.174	-.181	-.218	-.245	-.281	-.291	-.15	0
	0.9	-.388	-.399	-.418	-.434	-.461	-.478	-.495	-.525	-.565	-.624	-.682	-.35	0
	1.1	-.798	-.802	-.809	-.818	-.830	-.842	-.862	-.924	-.936	-.959	-.959	-.48	0
	1.5	-1.11	-1.10	-1.08	-1.07	-1.08	-1.08	-1.08	-1.09	-1.06	-1.01	-.96	-.48	0
	2.5	-1.17	-1.17	-1.17	-1.16	-1.16	-1.16	-1.16	-1.14	-1.12	-1.08	-.99	-.50	0
CN	0-0.5	0	.12	.22	.34	.50	.68	.86	1.24	1.67	2.15	2.96	6.50	5.65
	0.9	0	.06	.14	.27	.44	.62	.82	1.22	1.66	2.15	2.96	6.10	6.10
	1.1	0	.14	.27	.43	.63	.83	1.08	1.62	2.20	2.75	3.82	6.81	7.31
	1.5	0	.14	.28	.44	.63	.84	1.07	1.59	2.13	2.74	3.50	6.30	7.31
	2.5	0	.10	.21	.33	.47	.61	.76	1.12	1.51	1.96	2.63	5.80	7.15
CM	0-0.5	0	.053	.092	.090	.059	0	-.078	-.256	-.433	-.644	-1.21	-4.69	-5.36
	0.9	0	.040	.062	.090	.090	.038	-.013	-.080	-.150	-.160	-.17	-2.88	-4.83
	1.1	0	.086	.136	.123	.079	.044	-.054	-.241	-.428	-.550	-.71	-4.57	-5.79
	1.5	0	.021	.030	.023	.010	-.018	-.069	-.140	-.390	-.695	-.87	-3.60	-5.79
	2.5	0	.013	.017	.016	0	-.025	-.057	-.131	-.241	-.397	-.63	-3.90	-5.66
CNP (Body Fixed)	0-0.5	0	-.07	-.12	-.12	-.10	-.10	-.12	0	.25	.10	.60	-1.55	-1.20
	0.9	0	-.10	-.20	-.33	-.48	-.65	-.82	-1.28	-2.00	-1.50	-1.25	0	0
	1.1	0	0	0	-.11	-.20	-.27	-.37	-.60	-1.30	-1.50	-1.25	0	0
	1.5	0	.16	.35	.44	.37	.08	-.35	-.46	-.34	-.22	0	0	0
	2.5	0	.16	.32	.07	-.27	-.27	-.21	-.09	0	0	0	0	0
CMP	0-0.5	0	.07	.10	.08	.02	-.03	-.08	-.40	-.75	-.85	-.40	2.60	2.0
	0.9	0	.02	.04	.20	.42	.43	.37	.56	.85	1.42	1.48	0	0
	1.1	0	-.01	-.02	-.03	-.04	-.06	-.12	-.06	.80	1.42	1.48	0	0
	1.5	0	-.41	-.82	-.93	-.88	-.20	.64	.86	.78	.60	0	0	0
	2.5	0	-.36	-.48	-.13	-.49	-.48	-.41	-.21	0	0	0	0	0
CMQ	0-0.5	-19.3	-20.5	-22.0	-23.0	-24.5	-26.0	-27.2	-27.0	-26.8	-26.6	-26.3	-24.6	-23.0
	0.9	-22.5	-22.6	-22.6	-22.6	-22.7	-22.8	-22.8	-22.9	-23.0	-23.0	-23.0	-23.5	-24.0
	1.1	-37.0	-33.5	-30.0	-26.5	-22.5	-19.0	-15.0	-15.0	-15.0	-15.6	-17.0	-23.0	-29.0
	1.5	-49.0	-48.6	-48.2	-47.8	-47.4	-47.0	-46.6	-45.6	-44.8	-43.9	-42.5	-35.7	-29.0
	2.5	-24.0	-24.0	-24.0	-24.0	-24.0	-24.0	-24.0	-24.0	-24.0	-24.3	-24.5	-26.9	-29.0
CNR	0-0.5	-19.3	-20.5	-22.0	-23.0	-24.5	-26.0	-27.2	-27.0	-26.8	-26.6	-26.3	-18.6	-11.0
	0.9	-22.5	-22.5	-22.6	-22.6	-22.7	-22.8	-22.8	-22.9	-23.0	-23.0	-23.0	-17.5	-12.0
	1.1	-37.0	-33.5	-30.0	-26.5	-22.5	-19.0	-15.0	-15.0	-15.0	-15.6	-17.0	-15.8	-15.0
	1.5	-49.0	-48.6	-48.2	-47.8	-47.4	-47.0	-46.6	-45.6	-44.8	-43.9	-42.5	-28.7	-15.0
	2.5	-24.0	-24.0	-24.0	-24.0	-24.0	-24.0	-24.0	-24.0	-24.0	-24.3	-24.8	-19.5	-14.0
CMPR = CMPQ	0-0.5	0	0	0	0	0	0	0	0	0	0	0	0	0
	0.9	0	0	0	0	0	0	0	0	0	0	0	0	0
	1.1	0	0	0	0	0	0	0	0	0	0	0	0	0
	1.5	0	0	0	0	0	0	0	0	0	0	0	0	0
	2.5	0	0	0	0	0	0	0	0	0	0	0	0	0
CL x 10^3 (0.1 Deg Cant)	0-0.5	.30	.44	.56	.70	.82	.89	.97	.99	.86	.58	0	0	0
	0.9	.44	.56	.66	.76	.84	.91	.97	.97	.78	0	0	0	0
	1.1	.62	.79	.93	1.07	1.18	1.28	1.37	.94	.76	0	0	0	0
	1.5	.52	.66	.78	.90	.99	1.07	1.14	.68	.55	0	0	0	0
	2.5	.22	.28	.33	.38	.42	.45	.48	.38	.30	0	0	0	0
CLP	0-0.5	-.38	-.39	-.41	-.48	-.56	-.60	-.63	-.64	-.55	-.35	0	-.12	-.25
	0.9	-.34	-.36	-.40	-.45	-.51	-.53	-.50	-.28	-.20	0	0	-.22	-.45
	1.1	-.34	-.37	-.41	-.46	-.51	-.55	-.56	-.56	-.56	-.56	-.56	-.48	-.37
	1.5	-.35	-.38	-.43	-.47	-.52	-.57	-.62	-.62	-.62	-.62	-.62	-.43	-.23
	2.5	-.22	-.28	-.33	-.36	-.38	-.41	-.37	-.37	-.37	-.37	-.37	-.27	-.16
BODY-FIXED AERODYNAMIC COEFFICIENTS														
CLPH1	0-0.5	0	0	0	0	0	0	0	0	.012	-.015	-.025	0	0
	0.9	0	0	0	0	0	0	0	0	.005	0	-.005	0	0
	1.1	0	0	0	0	0	0	0	0	.005	0	-.005	0	0
	1.5	0	0	0	0	0	0	0	-.0007	.0006	.0185	-.0025	0	0
	2.5	0	0	0	0	-.0005	-.0012	-.0023	-.0002	.0040	-.0017	-.0094	0	0
CSF1	0-0.5	0	0	0	0	0	0	.004	.007	-.045	.028	.050	0	0
	0.9	0	0	0	0	0	0	.006	-.010	-.048	.021	.031	0	0
	1.1	0	0	0	0	0	0	.006	-.010	-.048	.021	.031	0	0
	1.5	0	0	0	0	0	.002	.003	-.024	.025	.090	.090	0	0
	2.5	0	0	0	0	0	0	0	.005	.019	.017	.028	0	0
CSM1	0-0.5	0	0	0	-.003	-.008	-.016	-.024	-.044	-.020	-.072	-.100	0	0
	0.9	0	0	0	0	0	0	-.01	-.026	.004	-.042	-.090	0	0
	1.1	0	0	0	0	0	0	-.01	-.026	.004	-.042	-.090	0	0
	1.5	0	0	0	0	0	0	0	.062	-.023	-.143	-.135	0	0
	2.5	0	0	0	0	0	0	0	-.015	-.045	-.042	-.062	0	0

Ref. area = $\pi d^2/4$. d= body diameter
Ref. length = d
cg location = 1.728 calibers from nose

APPENDIX B

RUN	ALPHA	CL	CD	CM	XCP	CS	CN	CX	MACH	RED
S-001	0.0	-0.0138	0.2169	0.1624	11.7594	-0.0056	0.1270	0.2169	0.1791	0.1005E+06
S-002	-1.00	-0.0482	0.2084	-0.0119	-0.2286	0.0008	0.0258	0.2075	0.1794	0.1006E+06
S-003	-2.00	-0.0789	0.2055	-0.1439	-1.6724	0.0009	0.0187	0.2026	0.1794	0.1006E+06
S-004	-3.00	-0.1220	0.2205	-0.0800	-0.5997	-0.0013	0.1304	0.2138	0.1797	0.1008E+06
S-005	-4.00	-0.1669	0.2360	-0.0361	-0.1975	-0.0032	0.0163	0.2238	0.1795	0.1007E+06
S-006	-5.00	-0.1995	0.2332	-0.2335	-1.0656	-0.0012	0.0184	0.2149	0.1793	0.1006E+06
S-007	-6.00	-0.2569	0.2551	-0.1740	-0.6168	0.0015	0.1051	0.2268	0.1792	0.1005E+06
S-008	-7.00	-0.3208	0.2763	-0.0928	-0.2636	0.0029	0.0952	0.2351	0.1789	0.1003E+06
S-009	-8.00	-0.3896	0.3015	-0.0112	-0.0262	0.0035	0.0887	0.2444	0.1786	0.1001E+06
S-010	-9.00	-0.4563	0.3133		-0.2188	0.0143	-0.1571	0.2381	0.1781	0.9985E+05
S-011	-10.00	-0.5179	0.3254		-0.4117	0.0151	-0.1578	0.2305	0.1779	0.9975E+05
S-012	-11.00	-0.6072	0.3563		0.4084	0.0243	-0.1294	0.2339	0.1775	0.9948E+05
S-013	-12.00	-0.6761	0.3895		-0.2663	0.0111	-0.0262	0.2404	0.1772	0.9935E+05
S-014	-13.00	-0.7644	0.4266		-0.3442	0.0206	-0.1200	0.2438	0.1770	0.9923E+05
S-015	-14.00	-0.8417	0.4596		-0.4093	0.0181	-0.1414	0.2424	0.1769	0.9917E+05
S-016	-15.00	-0.8724	0.5268		-0.4163	0.0311	-0.1988	0.2830	0.1763	0.9885E+05
S-017	-16.00	-1.0448	0.5575		-0.2288	0.0175	-0.1329	0.2479	0.1760	0.9875E+05
S-018	-17.00	-1.1289	0.6121		-0.3471	0.0214	-0.1721	0.2553	0.1756	0.9853E+05
S-019	-18.00	-1.1846	0.6536		-1.3363	0.0031	0.0159	0.2555	0.1753	0.9828E+05
S-020	-19.00	-1.3102	0.7401		-0.2285	0.0017	-0.0038	0.2732	0.1744	0.9782E+05
S-021	-20.00	-1.3603	0.7606		-0.5848	0.0100	0.0389	0.2495	0.1744	0.9779E+05

RUN	ALPHA	CL	CD	CM	XCP	CS	CN	CX	MACH	RED
S-022	-20.00	-1.3798	0.7627		-0.6188	0.0058	0.1265	0.2448	0.1744	0.9781E+05
S-023	-19.00	-1.3030	0.7345		-0.2535	0.0037	-0.1050	0.2703	0.1747	0.9798E+05
S-024	-18.00	-1.2241	0.6806		-0.0691	0.0145	-0.0889	0.2690	0.1753	0.9835E+05
S-025	-17.00	-1.1370	0.6226		-0.2186	0.0155	-0.0982	0.2630	0.1757	0.9854E+05
S-026	-16.00	-1.0436	0.5664		-0.1284	0.0191	-0.0683	0.2568	0.1764	0.9895E+05
S-027	-15.00	-0.9273	0.4996		-0.3102	0.0037	-0.1309	0.2426	0.1771	0.9935E+05
S-028	-14.00	-0.8512	0.4751		-0.1656	0.0166	-0.0772	0.2551	0.1775	0.9955E+05
S-029	-13.00	-0.7586	0.4299		-0.2946	0.0084	0.0258	0.2483	0.1779	0.9978E+05
S-030	-12.00	-0.6696	0.3908		-0.1149	0.0194	-0.1519	0.2431	0.1787	0.1002E+06
S-031	-11.00	-0.5913	0.3549		-0.2955	0.0125	0.0168	0.2356	0.1786	0.1002E+06
S-032	-10.00	-0.5323	0.3449		0.0100	0.0105	-0.1135	0.2472	0.1793	0.1005E+06
S-033	-9.00	-0.4485	0.3112	-0.0926	-0.1884	0.0094	-0.1066	0.2372	0.1792	0.1005E+06
S-034	-8.00	-0.3705	0.2861	-0.1151	-0.2830	0.0107	-0.0337	0.2317	0.1802	0.1010E+06
S-035	-7.00	-0.3045	0.2654	-0.1493	-0.4464	0.0108	-0.0213	0.2263	0.1801	0.1010E+06
S-036	-6.00	-0.2477	0.2495	-0.1779	-0.6532	0.0084	-0.0003	0.2222	0.1807	0.1013E+06
S-037	0.0	-0.0016	0.2078	0.0070	4.3677	-0.0048	0.0737	0.2078	0.1803	0.1017E+06
S-038	1.00	0.0375	0.2145	0.1274	-3.0932	0.0027	-0.0284	0.2138	0.1808	0.1013E+06
S-039	2.00	0.0734	0.2192	0.1404	-1.7322	0.0019	-0.1365	0.2165	0.1807	0.1013E+06
S-040	3.00	0.1151	0.2317	0.1849	-1.4555	0.0049	-0.0608	0.2253	0.1815	0.1024E+06
S-041	4.00	0.1579	0.2383	0.1036	-0.5948	0.0084	-0.1445	0.2267	0.1812	0.1022E+06
S-042	5.00	0.1993	0.2546	0.1627	-0.7370	0.0026	0.0138	0.2363	0.1813	0.1022E+06

RUN	ALPHA	CL	CD	CM	XCP	CS	CN	CX	MACH	RED
S-043	6.00	0.2554	0.2750	0.2003	-0.7083	0.0107	-0.1226	0.2468	0.1810	0.1021E+06
S-044	7.00	0.3131	0.2911	0.1144	-0.3304	0.0049	-0.2722	0.2508	0.1806	0.1019E+06
S-045	8.00	0.3679	0.3107	0.1952	-0.4789	0.0065	-0.2419	0.2565	0.1808	0.1020E+06
S-046	9.00	0.4311	0.3340	0.1953	-0.4086	-0.0005	-0.1550	0.2625	0.1804	0.1017E+06
S-047	10.00	0.5091	0.3670	0.1663	-0.2942	-0.0024	-0.0704	0.2730	0.1798	0.1017E+06
S-048	11.00	0.6011	0.3987	0.0354	-0.0532	0.0114	0.0159	0.2767	0.1786	0.1010E+06
S-049	12.00	0.6715	0.4434	0.1163	-0.1552	0.0064	-0.2806	0.2941	0.1787	0.1010E+06
S-050	13.00	0.7352	0.4798	0.1939	-0.2353	-0.0029	-0.2139	0.3021	0.1790	0.1012E+06
S-051	14.00	0.8250	0.5412	-0.8954	0.9613	-0.0019	0.0736	0.3256	0.1786	0.1010E+06
S-052	15.00	0.9075	0.5989	-0.9611	0.9340	0.0097	-0.0725	0.3339	0.1782	0.1007E+06
S-053	16.00	0.9797	0.6433	-0.9225	0.8244	0.0043	0.0307	0.3484	0.1782	0.1008E+06
S-054	17.00	1.0654	0.7093	-1.4673	1.1966	-0.0057	0.1380	0.3668	0.1775	0.1003E+06
S-055	18.00	1.1534	0.7733	-1.7825	1.3343	-0.0048	0.1329	0.3790	0.1769	0.9999E+05
S-056	19.00	1.3190	0.8092		1.1486	0.0033	0.0295	0.3357	0.1766	0.9979E+05
S-057	20.00	1.3003	0.9169		1.6214	-0.0049	0.1119	0.4169	0.1763	0.9960E+05
S-058	20.00	1.3070	0.9193		1.6011	0.0033	0.1228	0.4169	0.1763	0.9985E+05
S-059	19.00	1.3001	0.7998		1.1307	-0.0050	0.1735	0.3330	0.1774	0.1004E+06
S-060	18.00	1.1598	0.7747	-2.0256	1.5089	-0.0014	0.1683	0.3764	0.1774	0.1004E+06
S-061	17.00	1.0709	0.7082	-1.6342	1.3274	-0.0106	0.2769	0.3642	0.1781	0.1009E+06
S-062	16.00	0.9940	0.6485	-1.3512	1.1913	0.0045	0.0720	0.3494	0.1787	0.1012E+06
S-063	15.00	0.9116	0.5895	-1.2003	1.1618	-0.0001	0.0748	0.3335	0.1793	0.1015E+06

RUN	ALPHA	CL	CD	CM	XCP	CS	CN	CX	MACH	RED
S-064	14.00	0.8268	0.5397	-0.9317	0.9988	0.0174	-0.1292	0.3236	0.1796	0.1017E+06
S-065	13.00	0.7536	0.4826	-0.2087	0.2477	0.0035	-0.2521	0.3007	0.1801	0.1019E+06
S-066	12.00	0.6693	0.4363	-0.0748	0.1003	0.0034	-0.3198	0.2876	0.1802	0.1020E+06
S-067	11.00	0.5886	0.3998	0.1372	-0.2097	0.0126	-0.0368	0.2802	0.1805	0.1022E+06
S-068	10.00	0.5133	0.3642	0.1118	-0.1966	0.0028	-0.2045	0.2696	0.1809	0.1024E+06
S-069	9.00	0.4384	0.3350	0.1683	-0.3467	0.0002	-0.1682	0.2623	0.1817	0.1028E+06
S-070	8.00	0.3761	0.3132	0.1787	-0.4296	0.0012	-0.1758	0.2578	0.1816	0.1028E+06
S-071	7.00	0.3145	0.2890	0.1141	-0.3285	0.0011	-0.3140	0.2485	0.1828	0.1035E+06
S-072	6.00	0.2593	0.2714	0.1200	-0.4194	0.0024	-0.0990	0.2428	0.1828	0.1035E+06
S-073	5.00	0.2029	0.2519	0.1363	-0.6080	-0.0018	-0.0563	0.2332	0.1832	0.1036E+06
S-074	4.00	0.1590	0.2371	0.1075	-0.6137	-0.0011	-0.1028	0.2254	0.1832	0.1036E+06
S-075	3.00	0.1178	0.2352	0.2626	-2.0209	0.0024	-0.0996	0.2287	0.1832	0.1036E+06
S-076	2.00	0.0735	0.2187	0.1845	-2.2756	0.0007	-0.1647	0.2160	0.1837	0.1039E+06
S-077	1.00	0.0363	0.2124	0.1383	-3.4525	0.0010	-0.0898	0.2118	0.1837	0.1039E+06
S-078	0.0	-0.0020	0.2069	0.0607	29.6171	0.0002	-0.0745	0.2069	0.1833	0.1037E+06
S-079	-1.00	-0.0375	0.1993	-0.0774	-1.8886	0.0008	-0.0858	0.1986	0.1838	0.1040E+06
S-080	-2.00	-0.0821	0.2149	0.0300	0.3349	0.0008	-0.1009	0.2119	0.1832	0.1037E+06
S-081	-3.00	-0.1145	0.2136	-0.1350	-1.0753	-0.0004	0.0058	0.2073	0.1835	0.1038E+06
S-082	-4.00	-0.1527	0.2215	-0.1820	-1.0849	-0.0026	-0.0688	0.2103	0.1823	0.1040E+06
S-083	-5.00	-0.2129	0.2501	-0.0087	-0.0373	-0.0042	-0.0632	0.2306	0.1821	0.1039E+06
S-084	-6.00	-0.2544	0.2525	-0.1536	-0.5497	-0.0012	-0.0157	0.2246	0.1818	0.1037E+06

RUN	ALPHA	CL	CD	CM	XCP	CS	CN	CX	MACH	RED
S-085	-7.00	-0.3169	0.2724	-0.0818	-0.2353	-0.0014	-0.0315	0.2318	0.1816	0.1036E+06
S-086	-8.00	-0.3841	0.2997	0.0155	0.0363	-0.0004	-0.0389	0.2426	0.1814	0.1035E+06
S-087	0.0	0.0032	0.1754	0.0160	-4.9553	0.0012	-0.0119	0.1754	0.3643	0.2080E+06
S-088	2.00	0.0720	0.1948	0.1404	-1.7871	0.0017	-0.0399	0.1922	0.3646	0.2082E+06
S-089	4.00	0.1614	0.2196	0.1999	-1.1341	-0.0008	-0.0231	0.2078	0.3644	0.2080E+06
S-090	6.00	0.2677	0.2529		-1.6834	0.0032	-0.0245	0.2235	0.3650	0.2083E+06
S-091	8.00	0.3722	0.2932	0.2783	-0.6798	0.0008	-0.0396	0.2386	0.3647	0.2081E+06
S-092	10.00	0.4920	0.3469	0.2805	-0.5149	-0.0033	-0.0227	0.2562	0.3648	0.2081E+06
S-093	12.00	0.6395	0.4307	0.2520	-0.3524	-0.0027	-0.0751	0.2883	0.3621	0.2067E+06
S-094	14.00	0.6601	0.5596	0.0810	-0.1044	0.0003	0.0069	0.3833	0.3608	0.2057E+06
S-095	12.00	0.6424	0.4332	0.2318	-0.3226	-0.0042	-0.0633	0.2901	0.3643	0.2077E+06
S-096	10.00	0.5004	0.3522	0.2589	-0.4674	0.0063	-0.0478	0.2599	0.3648	0.2079E+06
S-097	8.00	0.3705	0.2915	0.2538	-0.6229	-0.0004	-0.0292	0.2371	0.3681	0.2098E+06
S-098	6.00	0.2496	0.2489	0.2687	-0.9797	0.0026	-0.0191	0.2214	0.3698	0.2108E+06
S-099	4.00	0.1567	0.2165	0.1934	-1.1281	0.0004	-0.0274	0.2050	0.3709	0.2114E+06
S-100	2.00	0.0740	0.1936	0.1239	-1.5354	0.0034	-0.0493	0.1909	0.3719	0.2119E+06
S-101	0.0	0.0054	0.1769	0.0087	-1.6088	-0.0046	0.0011	0.1769	0.3721	0.2120E+06
S-102	-2.00	-0.0644	0.1868	-0.1016	-1.4334	-0.0062	-0.0048	0.1844	0.3729	0.2125E+06
S-103	0.0	0.0014	0.1779	0.0265	-19.2590	0.0036	-0.0215	0.1779	0.3647	0.2077E+06
S-104	-2.00	-0.0645	0.1861	-0.0975	-1.3736	-0.0020	-0.0098	0.1837	0.3648	0.2078E+06
S-105	-4.00	-0.1615	0.2086	-0.1563	-0.8897	0.0020	-0.0210	0.1968	0.3653	0.2079E+06

RUN	ALPHA	CL	CD	CM	XCP	CS	CN	CX	MACH	RED
S-106	-5.00	-0.2137	0.2217	-0.1899	-0.8180	0.0081	-0.0407	0.2022	0.3658	0.2083E+06
S-107	-6.00	-0.2722	0.2368	-0.2065	-0.6991	0.0101	-0.0284	0.2070	0.3671	0.2090E+06
S-108	-4.00	-0.1670	0.2115	-0.1409	-0.7767	0.0110	-0.0552	0.1994	0.3685	0.2097E+06
S-109	-2.00	-0.0728	0.1900	-0.0710	-0.8937	0.0020	-0.0239	0.1874	0.3702	0.2106E+06
S-110	0.0	0.0056	0.1759	0.0060	-1.0871	0.0039	-0.0205	0.1759	0.3713	0.2113E+06
S-111	2.00	0.0781	0.1961	0.1151	-1.3556	-0.0017	-0.0216	0.1932	0.3711	0.2111E+06

F I G U R E S

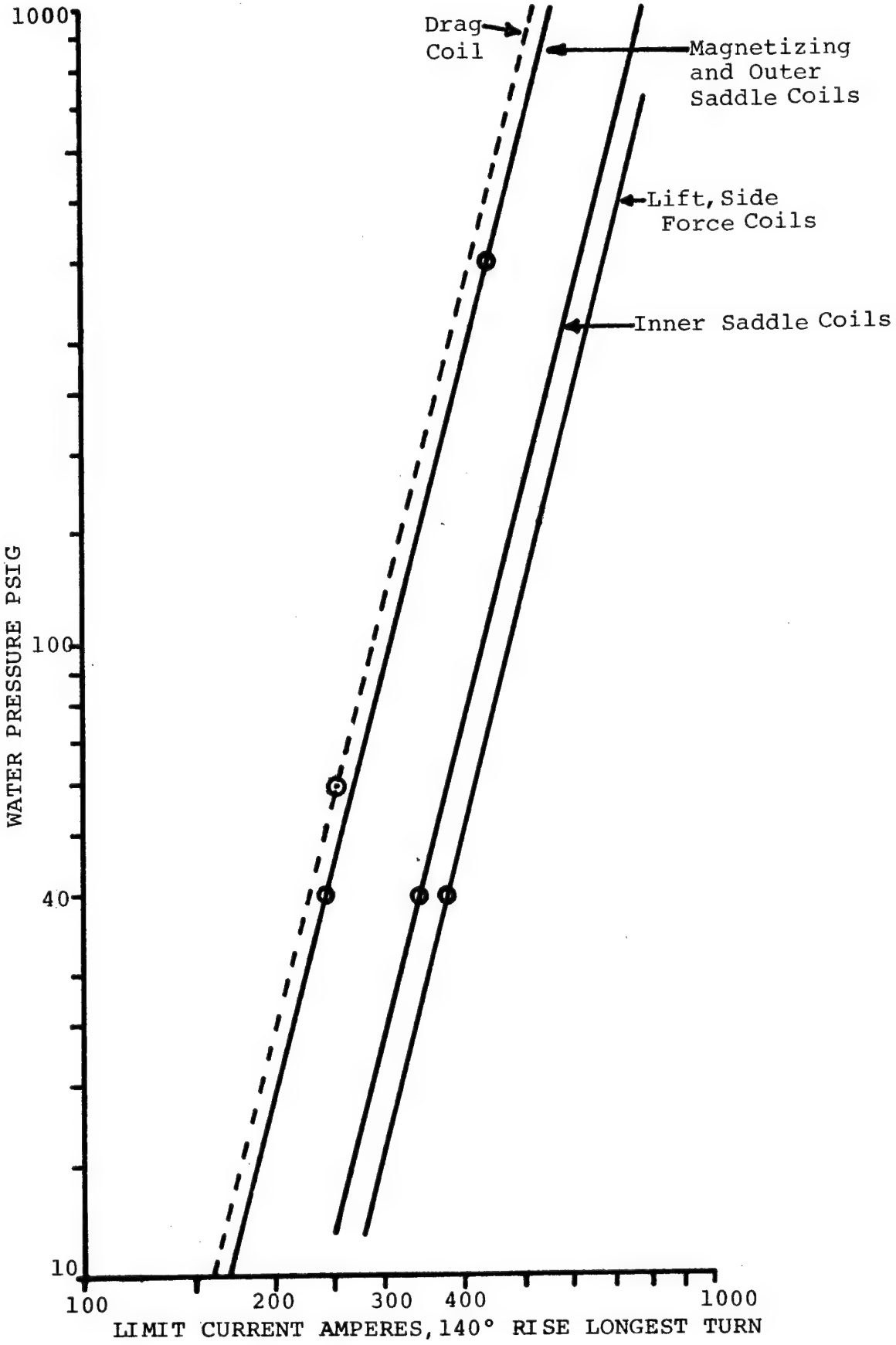

Figure 1 NASA Balance; Current Limits

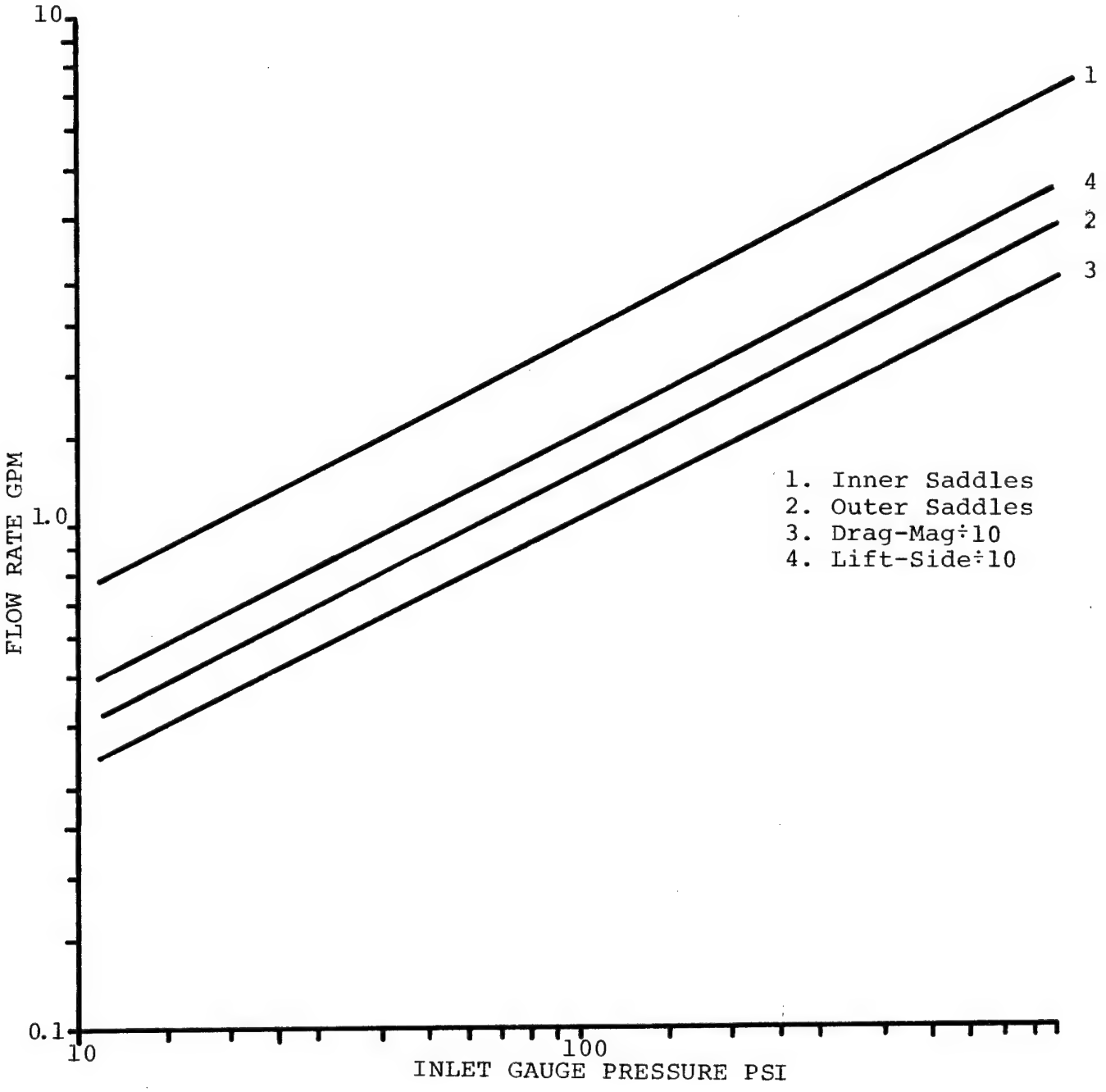

Figure 2 NASA Balance Water Demand by Circuit All Layers

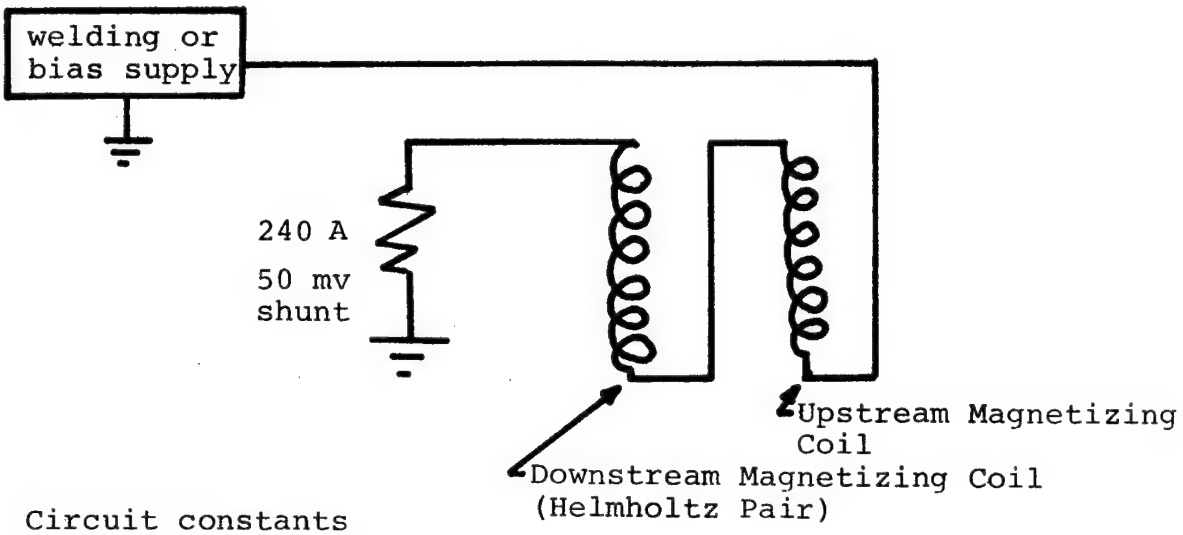

Circuit constants

R_{DC} = 2.0 ohm

$\frac{L}{R}$ = .18 sec.

L_{TOTAL} = .36 h

Energy @ 300A = 1600 Joules

N = 800 turns

Present Limit - about 200 amps. Decision based on probable coil damage

Figure 3 Circuit for Magnetizing Coils

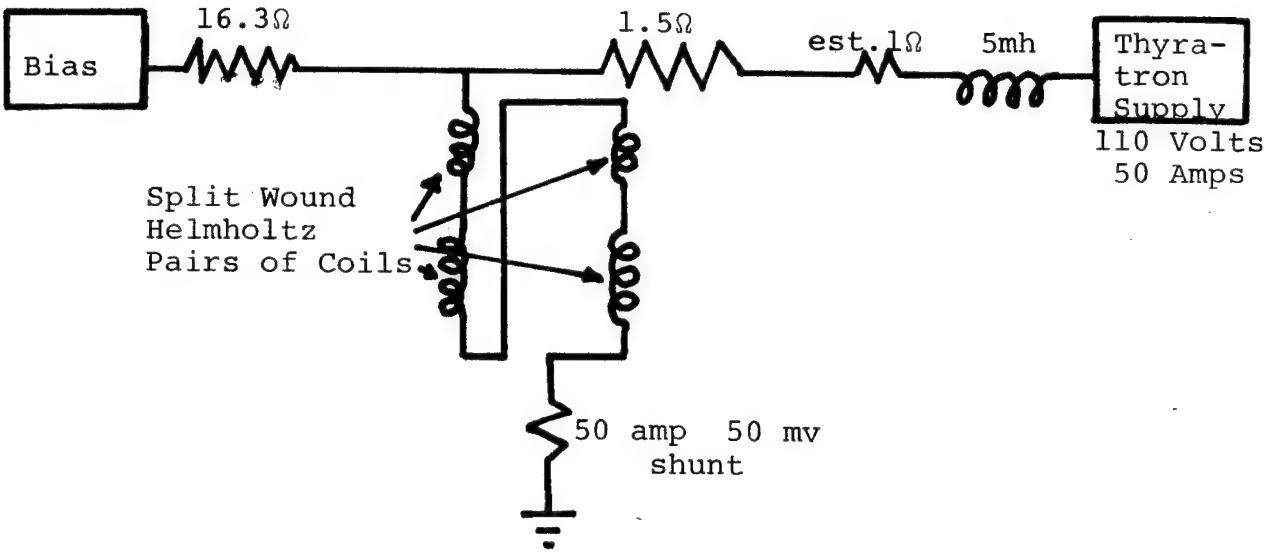

Coil Constants

R = 2.0 ohm

N = 800 turns

L = .16h

E = 720 Joules at 300 amps

Circuit Constants

L_{Total} = .165h R_{Total} = 3.6Ω $\frac{L}{R}$ = .046 sec.

Present Limit - Power Supply +40 -10 amperes

Figure 4 Drag Circuit

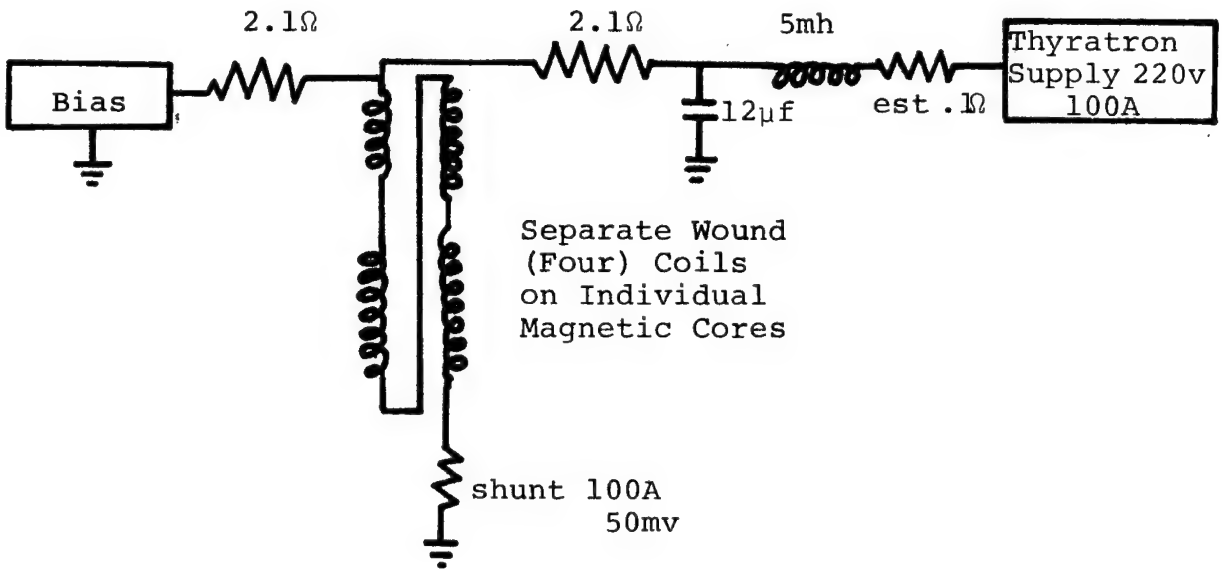

Coil Constants

R = 1Ω N = 1160 turns

L = 400 mh E = 1800 Joules at 300A

Circuit Constants

L = .405 R = 3.2 $\frac{L}{R}$ = .125 sec.

Present Limit - Power Supply $\pm$ 50 amps

Some assymetry possible with bias adjustment

Figure 5 Lift Circuit

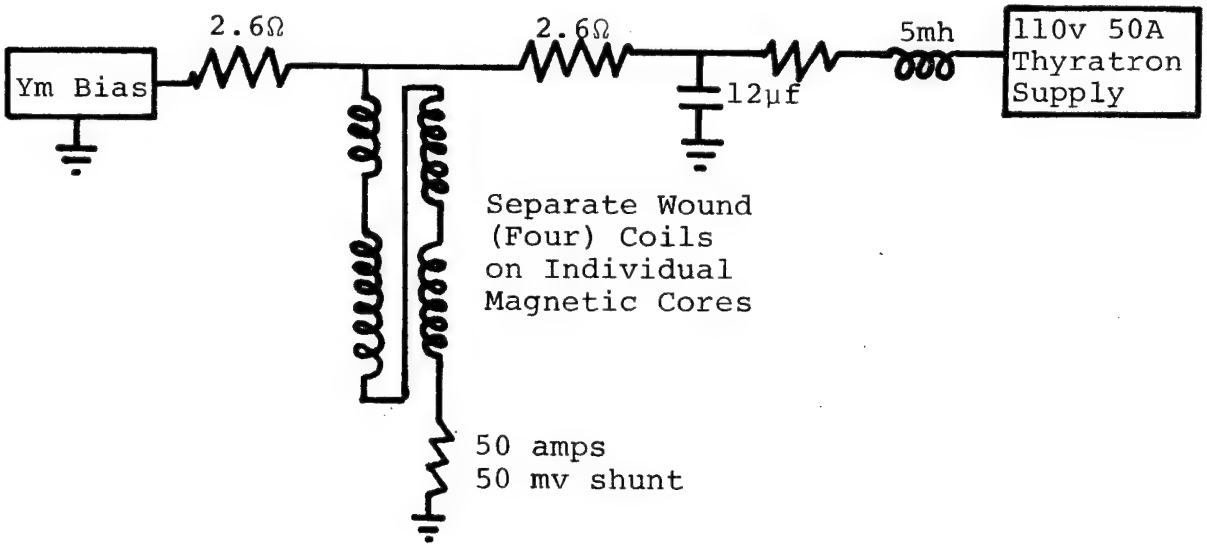

Coil Constants

R = 1Ω N = 1160 turns

L = 400 mh E = 1800 Joules @ 300A

Circuit Constants

L = .405h R = 3.6Ω $\frac{L}{R}$ = .110 sec.

Present Limit - Power Supply $\pm$ 25 amps

Figure 6 Side Force Circuit

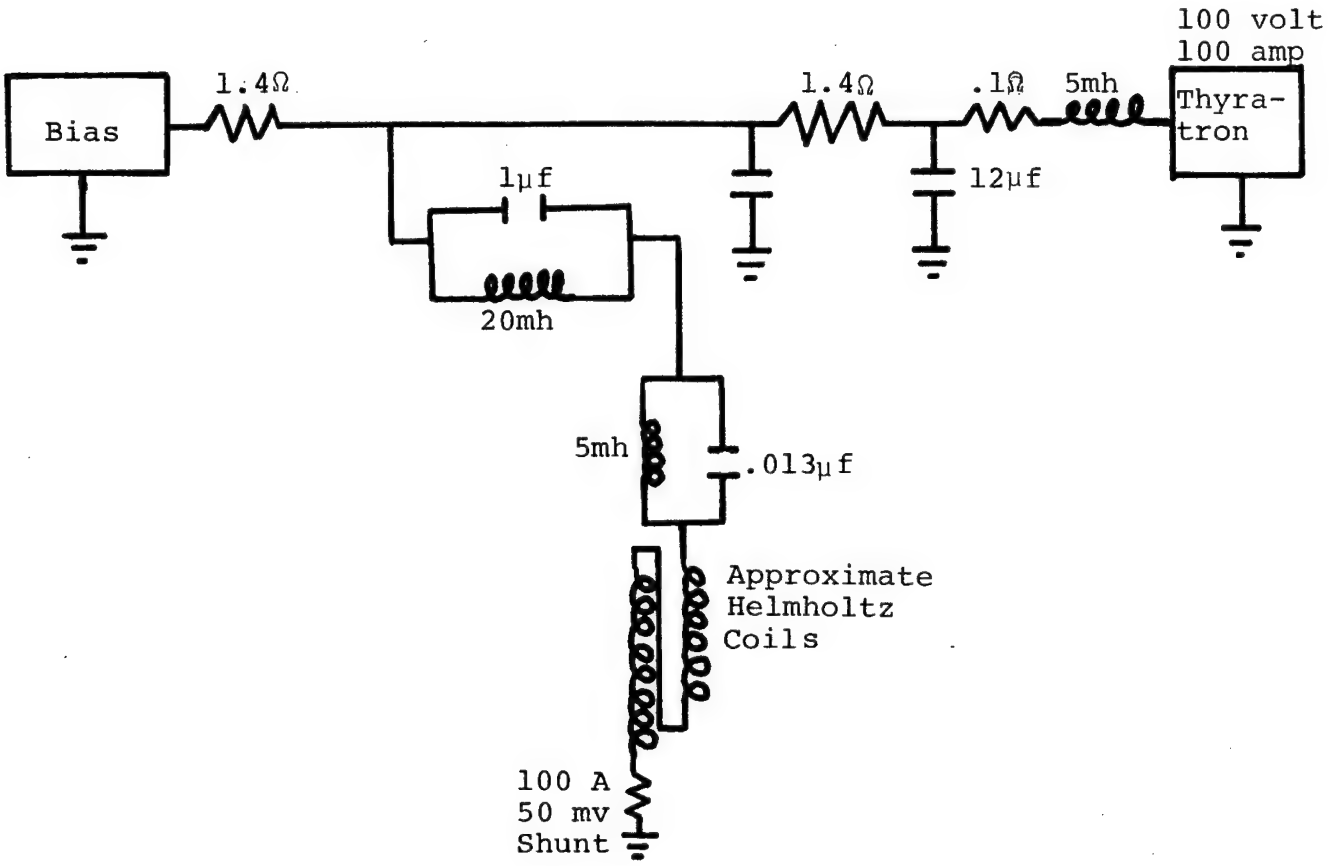

Coil Constants

R = .44Ω

L = 17 mh

N = 266 turns

E = 765 Joules at 300A

$B_z = 3.5\ I_z$

Circuit Constants

L = 47 mh R = 2.2 Ohms $\frac{L}{R}$ = .021 sec.

Present Limit - Power Supply ± 50 amps

Figure 7 Outer Saddle Circuit

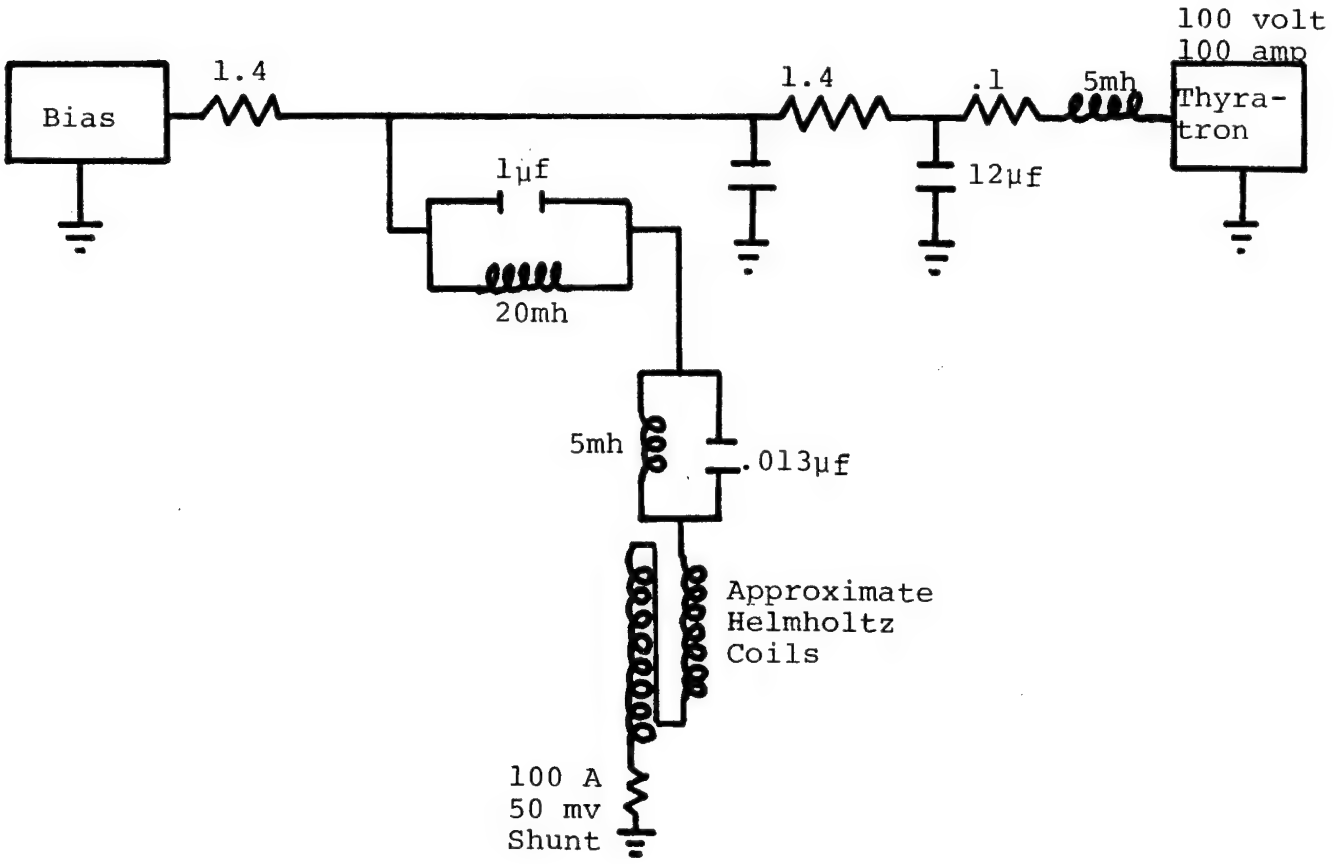

Coil Constants

R = .24Ω

E = 360 Joules @300 Amps

L = 8 mh

$B_y = 3.8\ I_y$

Circuit Constants

L = 38 mh

R = 2.0 ohms

$\frac{L}{R}$ = .019 sec

Present Limit - Power Supply ± 50 amps

Figure 8 Inner Saddle Circuit

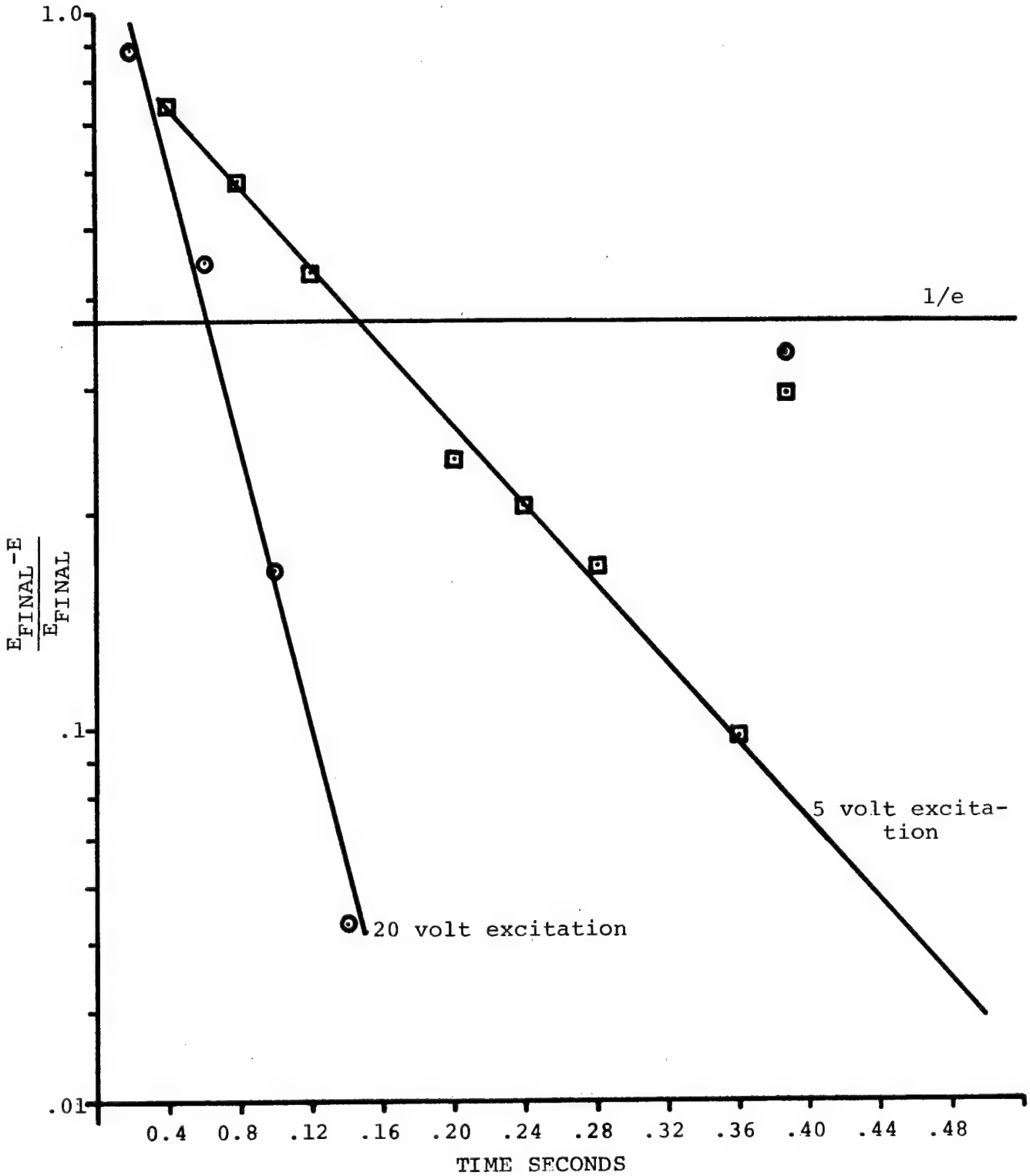

Figure 9 Armature Voltage - Time Response of Generator 1

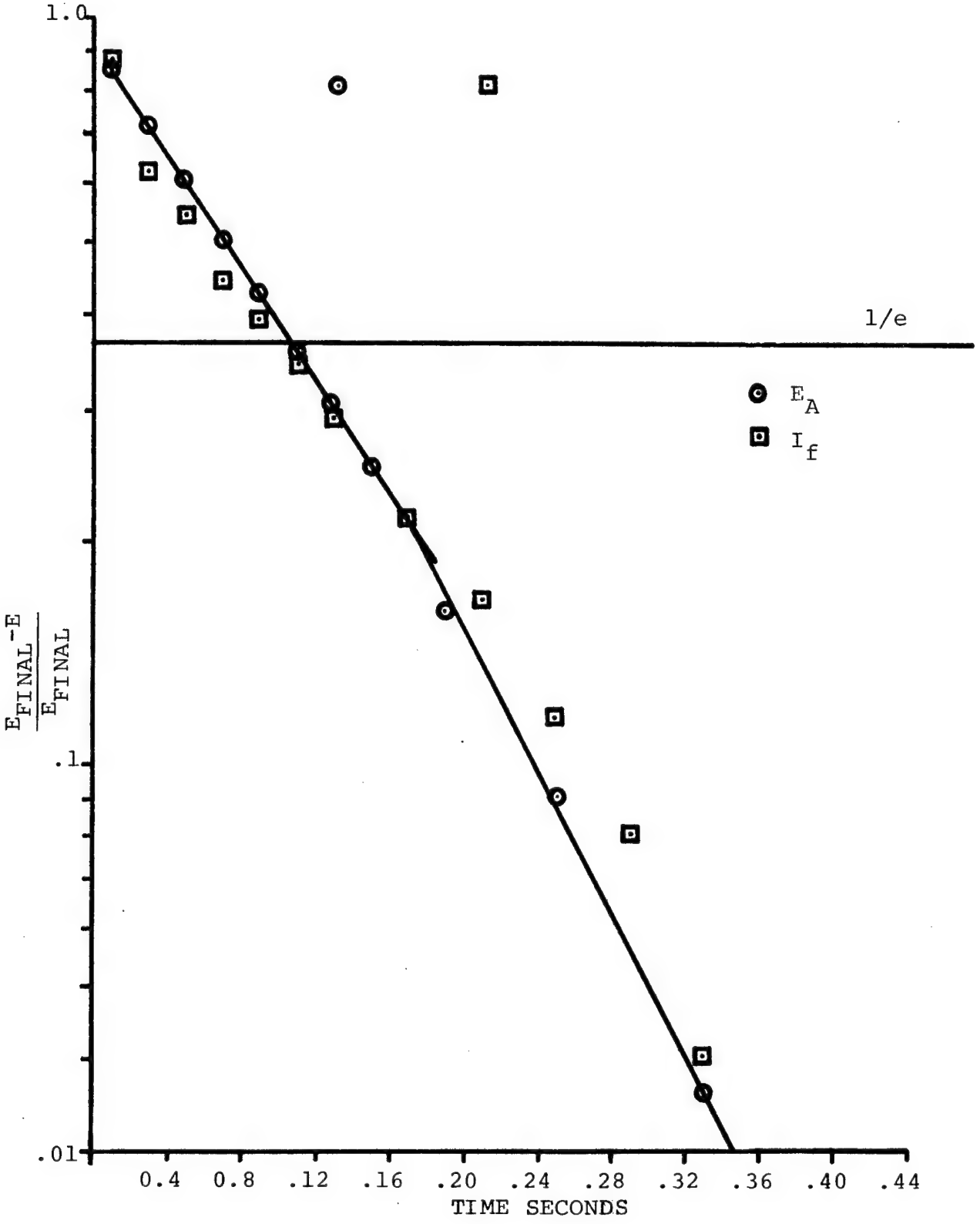

Figure 10 Field Current and Armature Voltage Time Response of Generator 1 at 10 volts Field Excitation

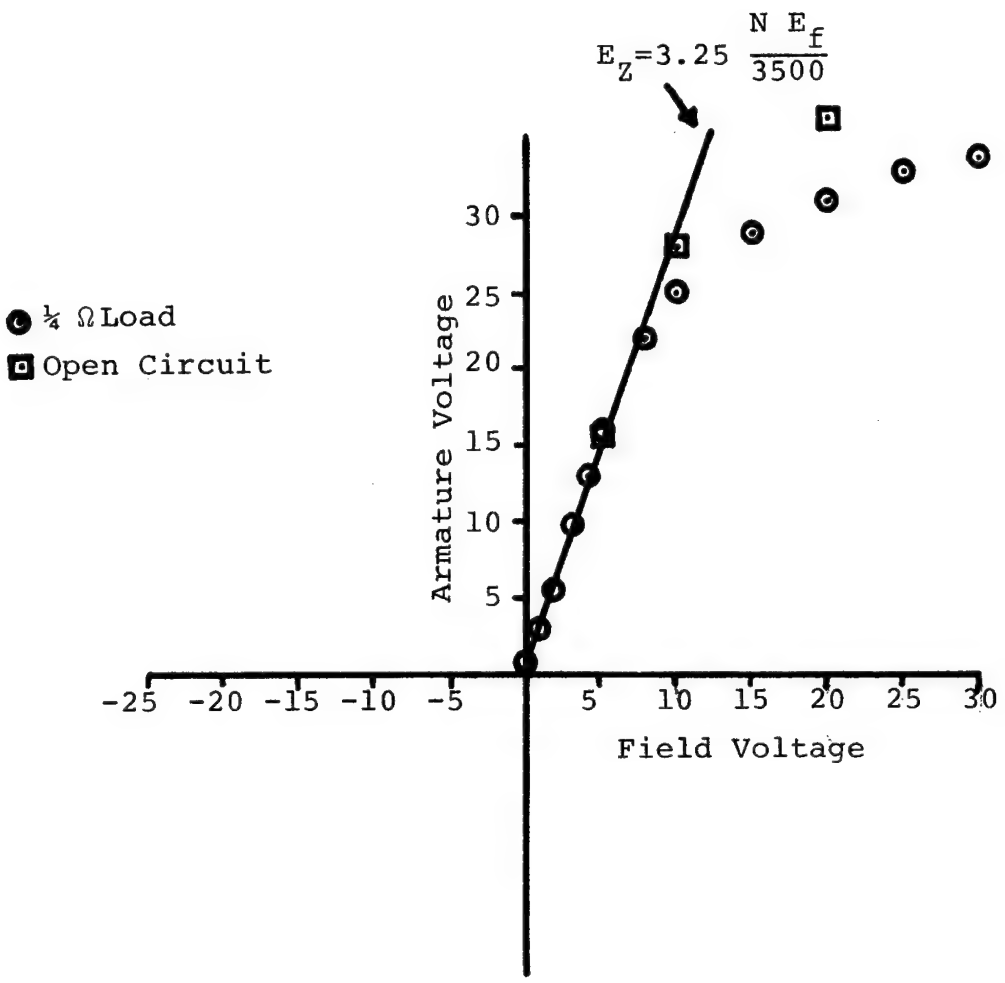

Figure 11 Generator 1 D.C. Output at 3500 rpm

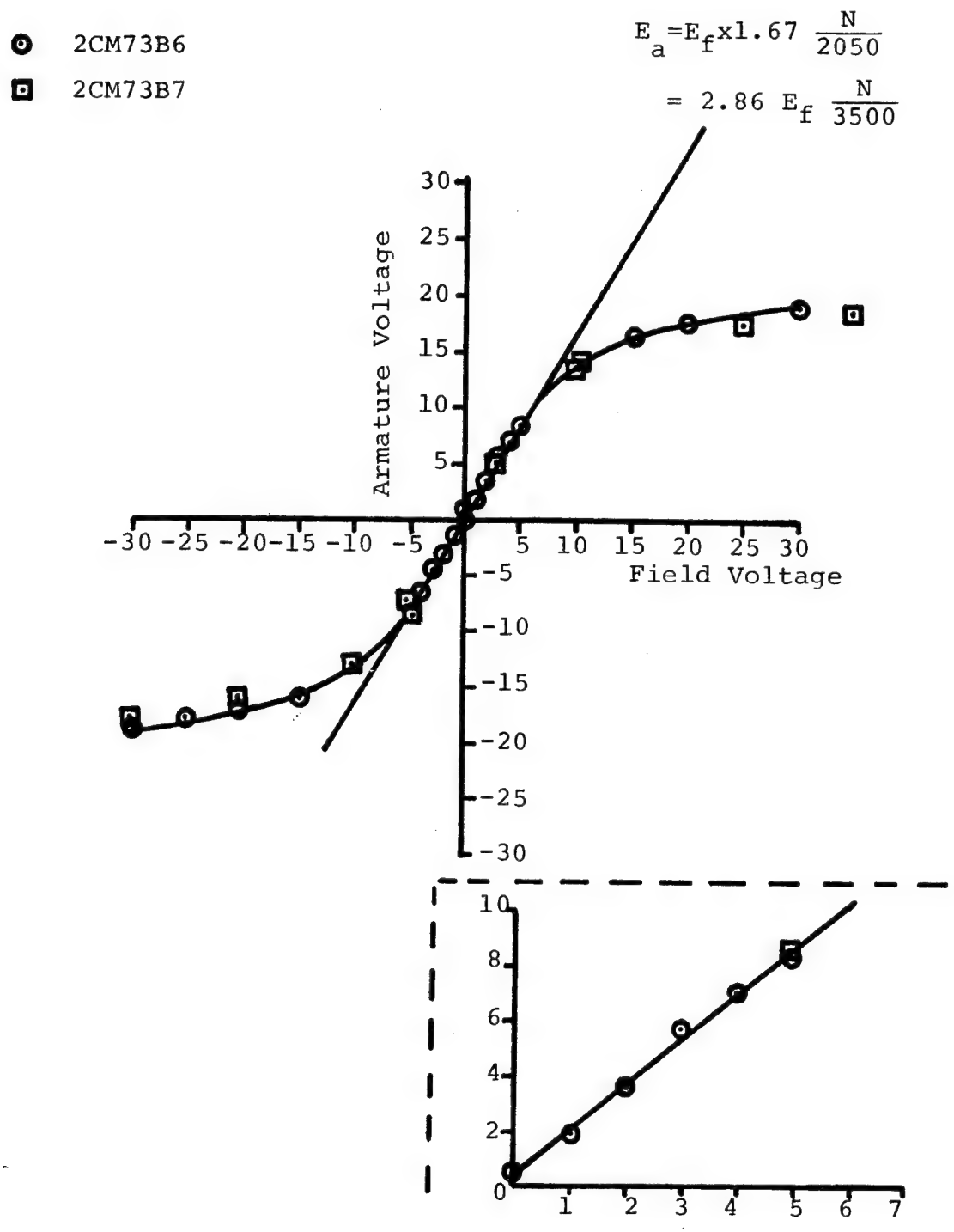

Figure 12 Generator 2 (Type R.1) D.C. Output at 250 rpm

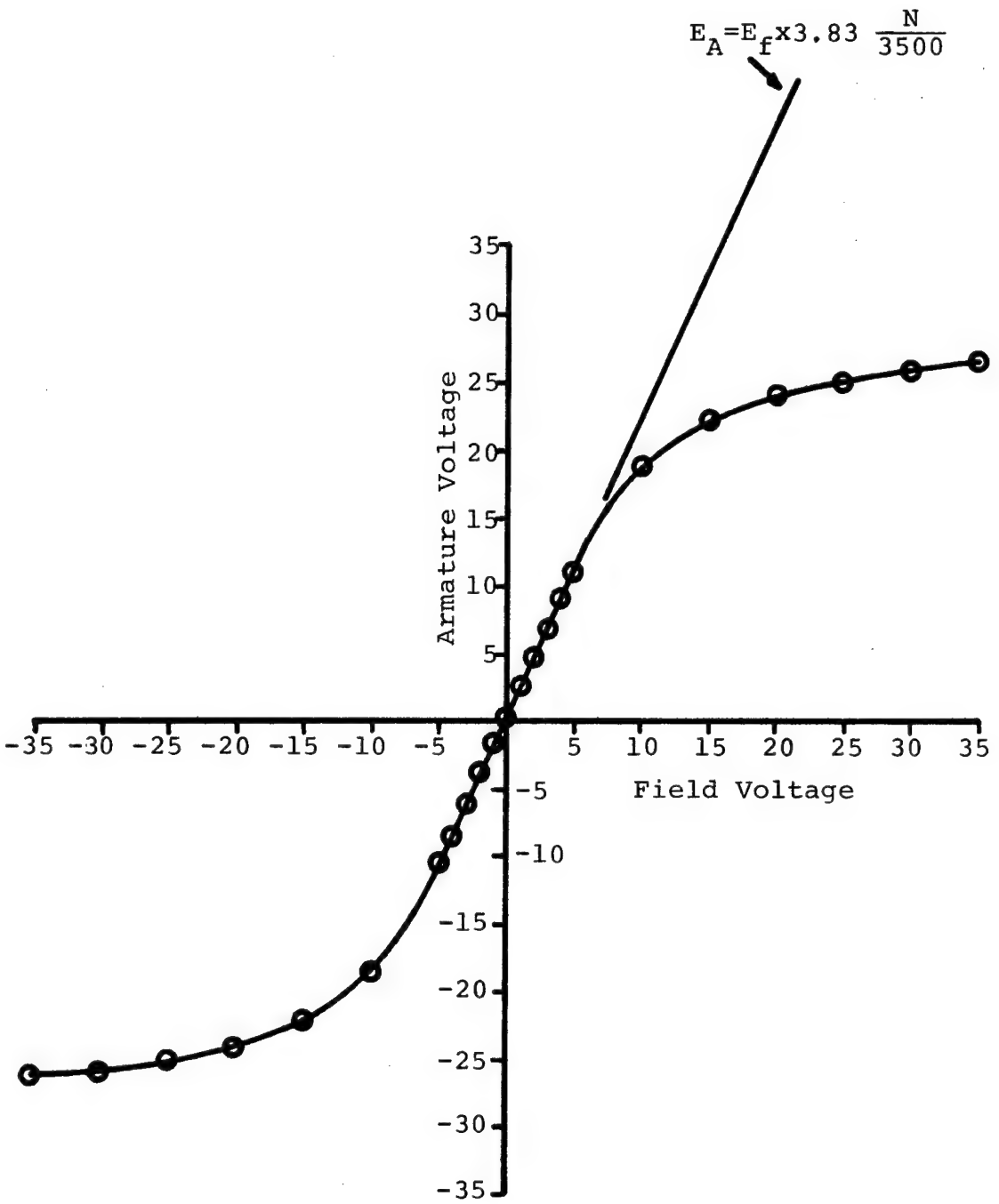

Figure 13 Generator 3 (Type A-45 J-244)
D.C. Output at 2000 rpm

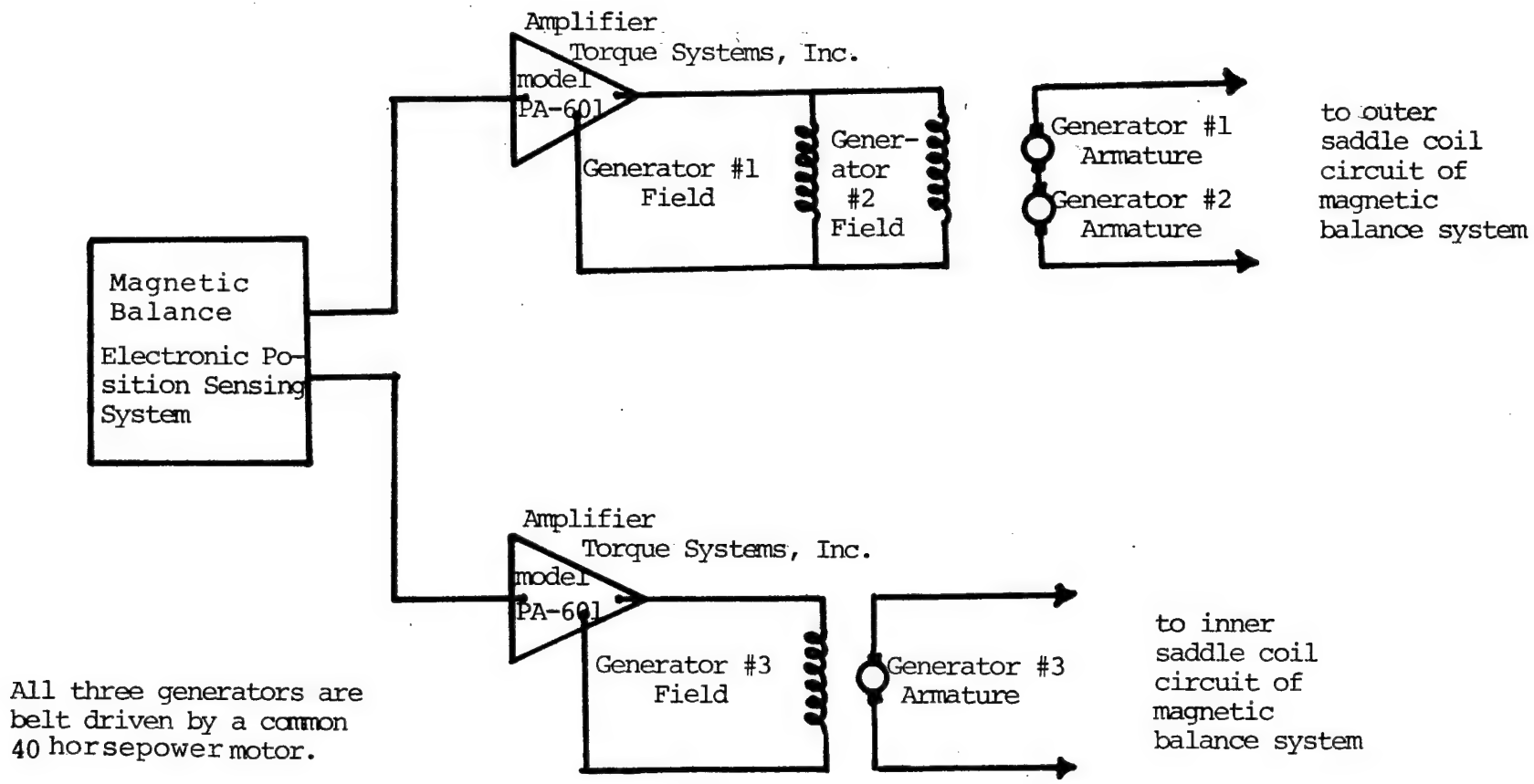

Figure 14 Block Diagram of Power Supply

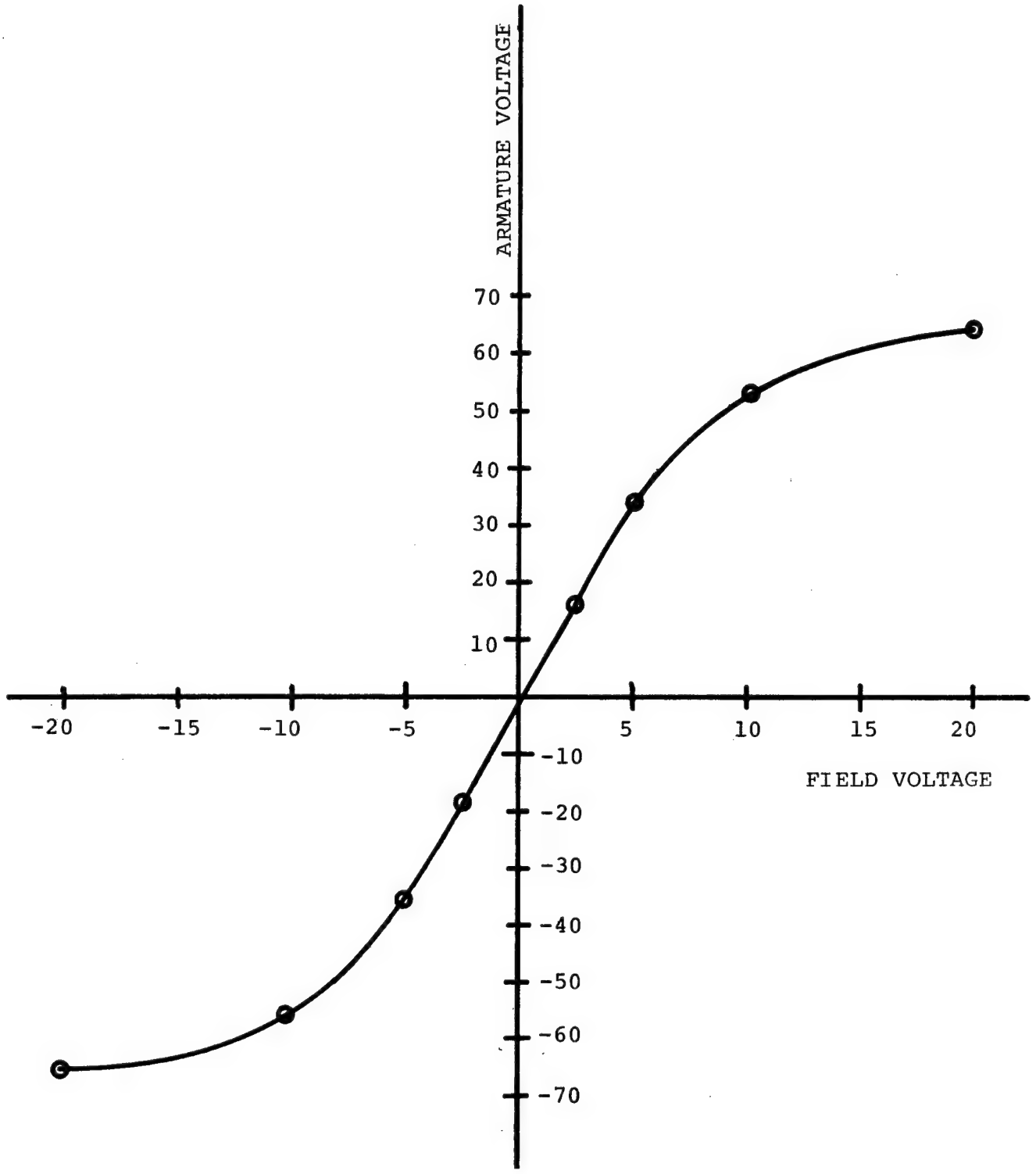

Figure 15 Generator D.C. Output

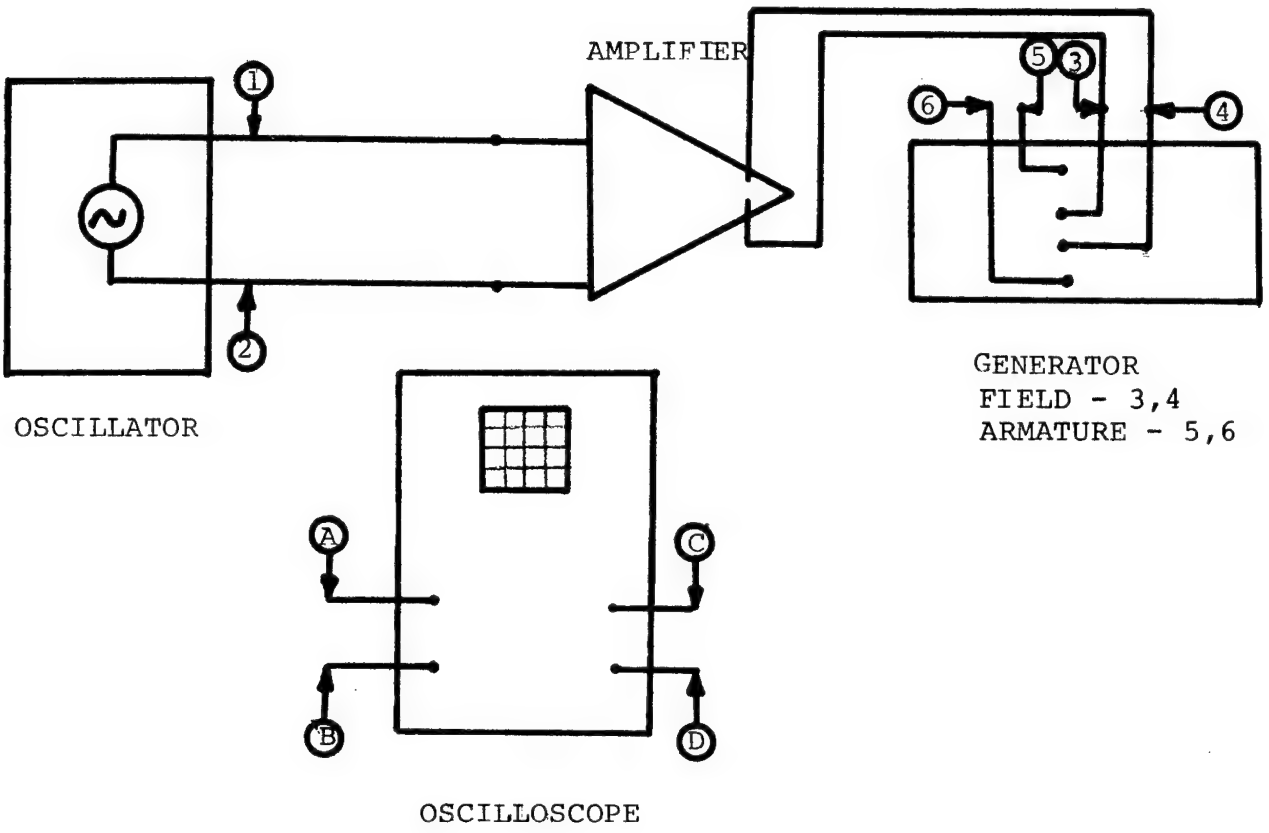

Figure 16 Block Diagram of Frequency Response Test Apparatus

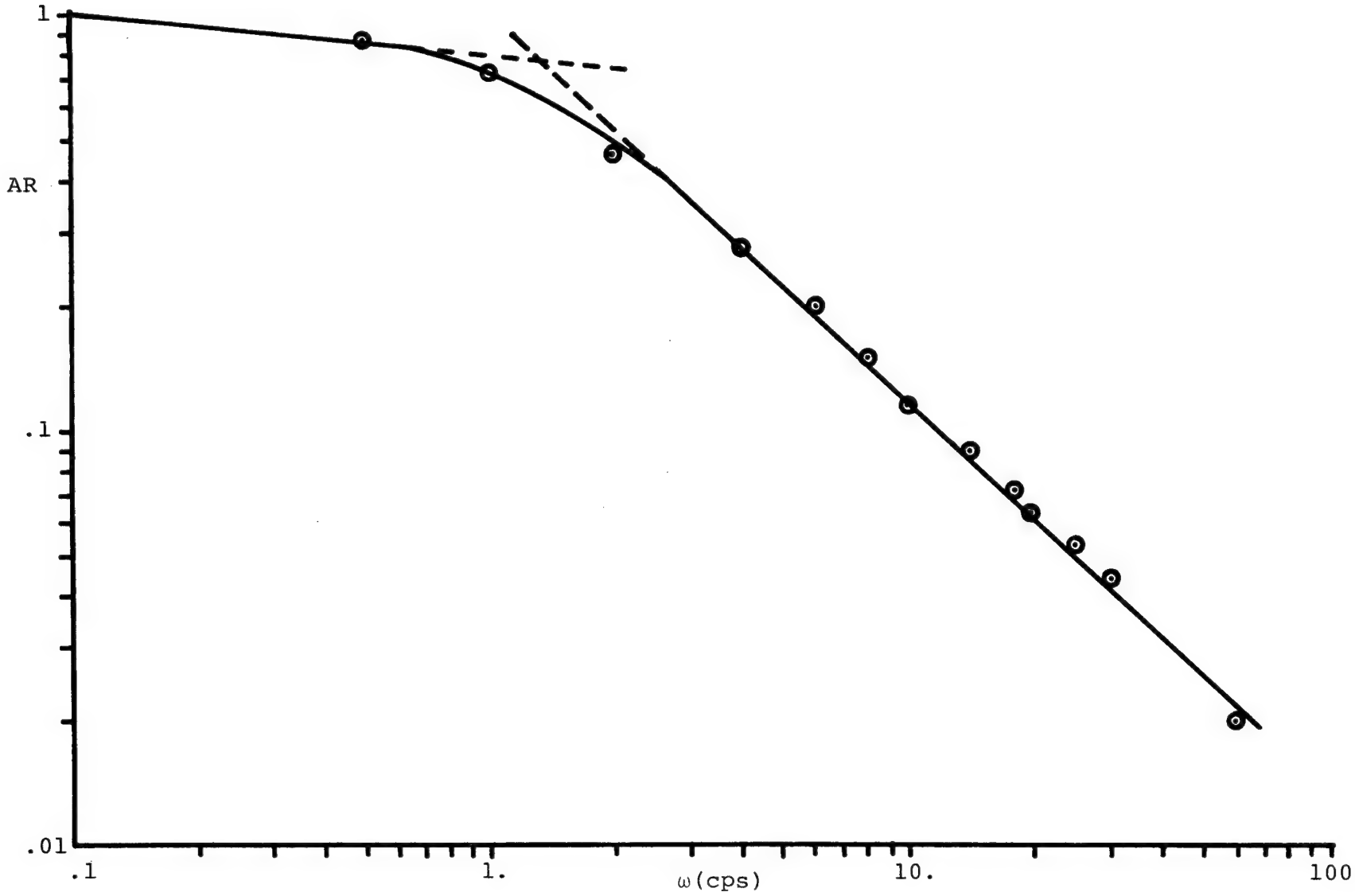

Figure 17 Frequency Response for E_F=2.5 Volts

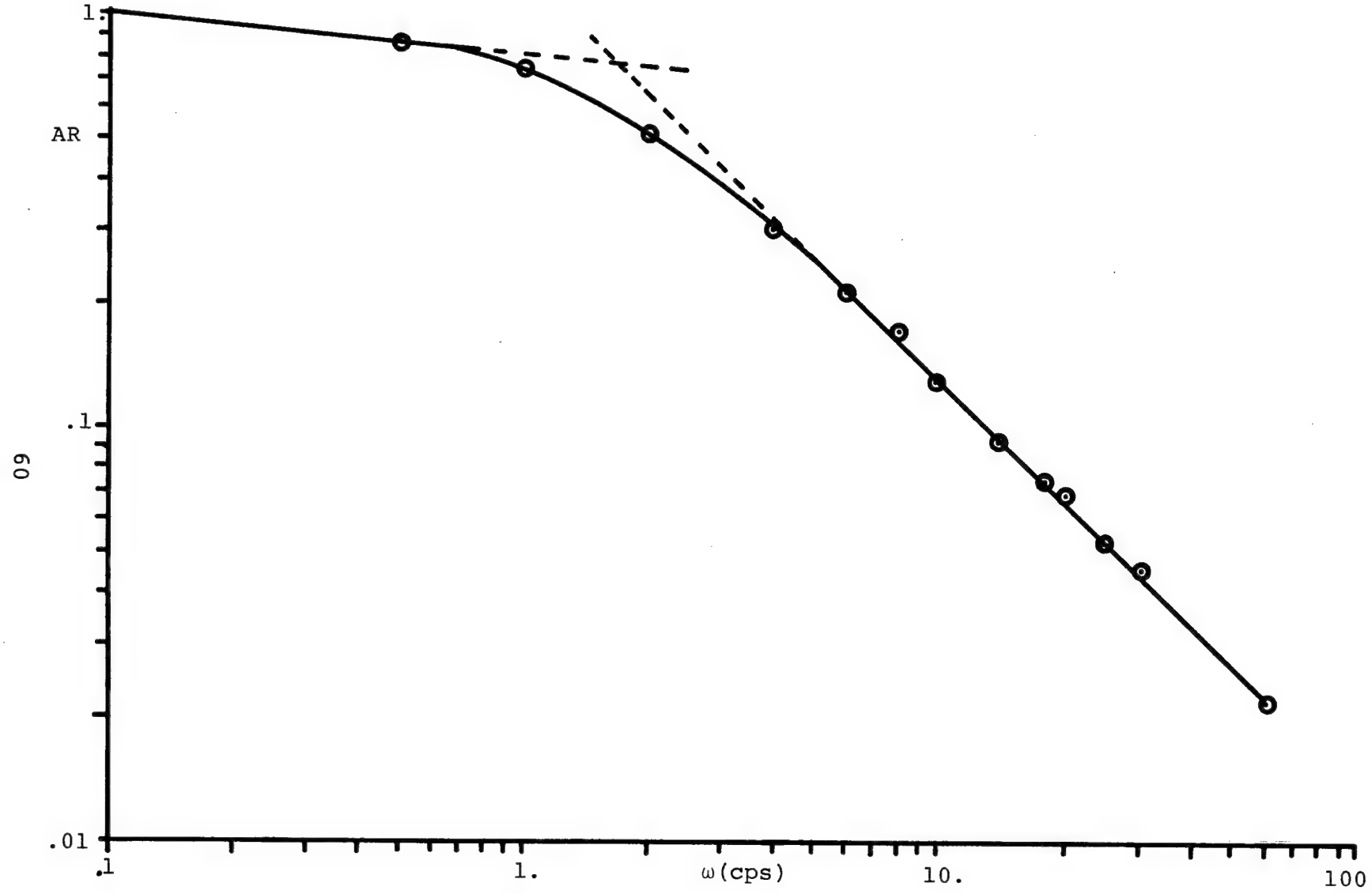

Figure 18 Frequency Response for E_F=5.0 Volts

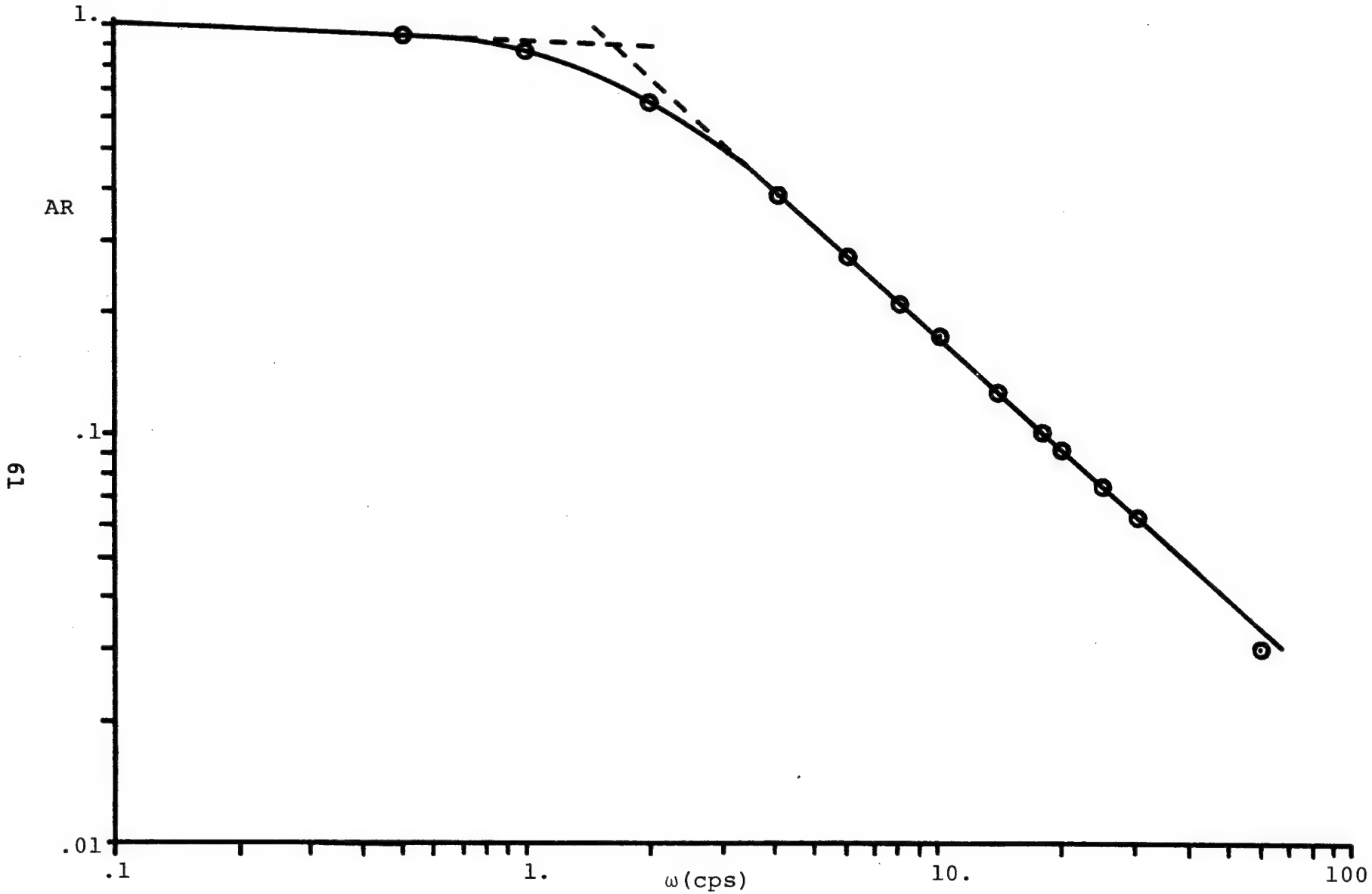

Figure 19 Frequency Response for E_F=10.0 Volts

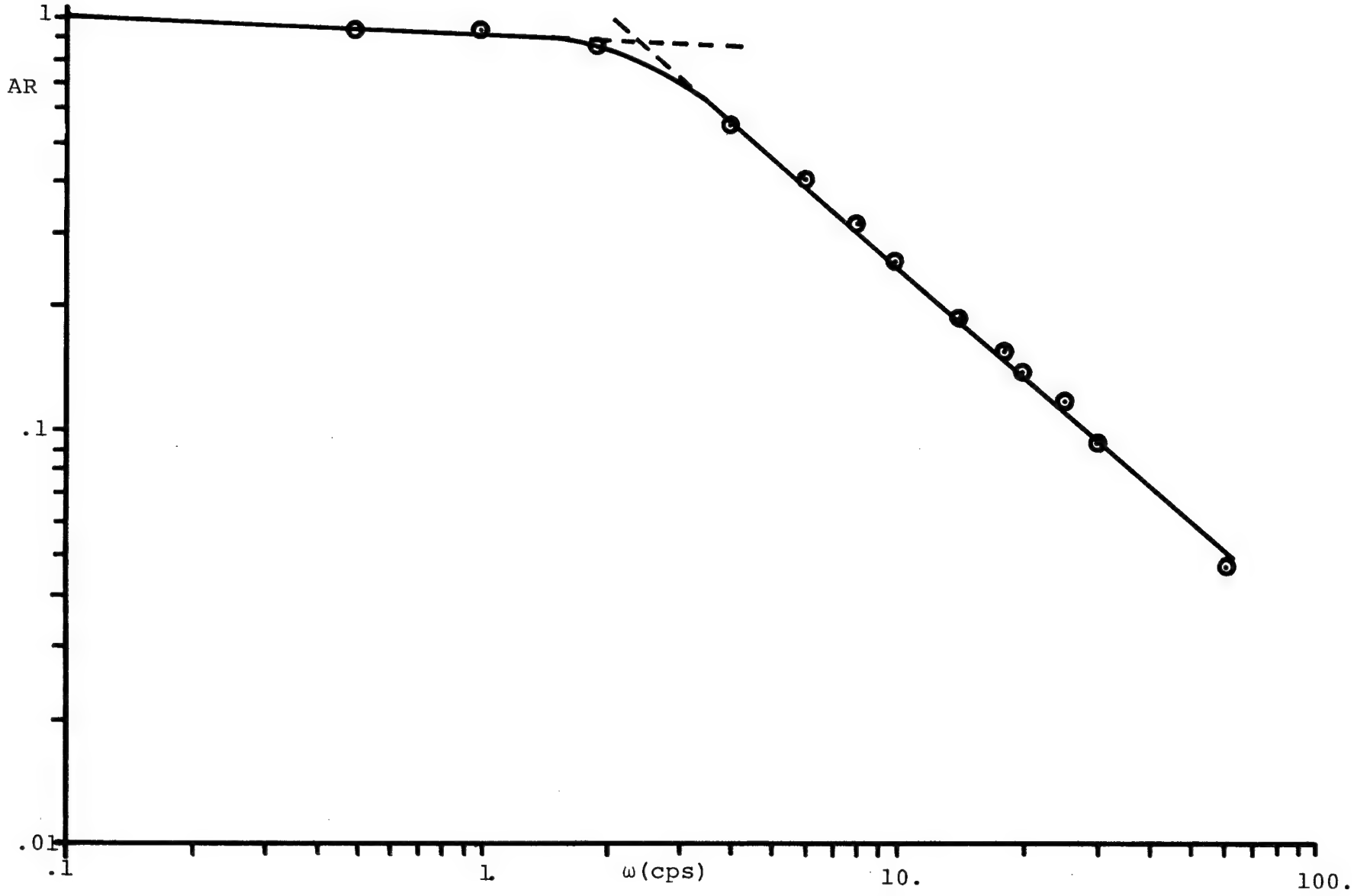

Figure 20 Frequency Response for E_F=20.0 Volts

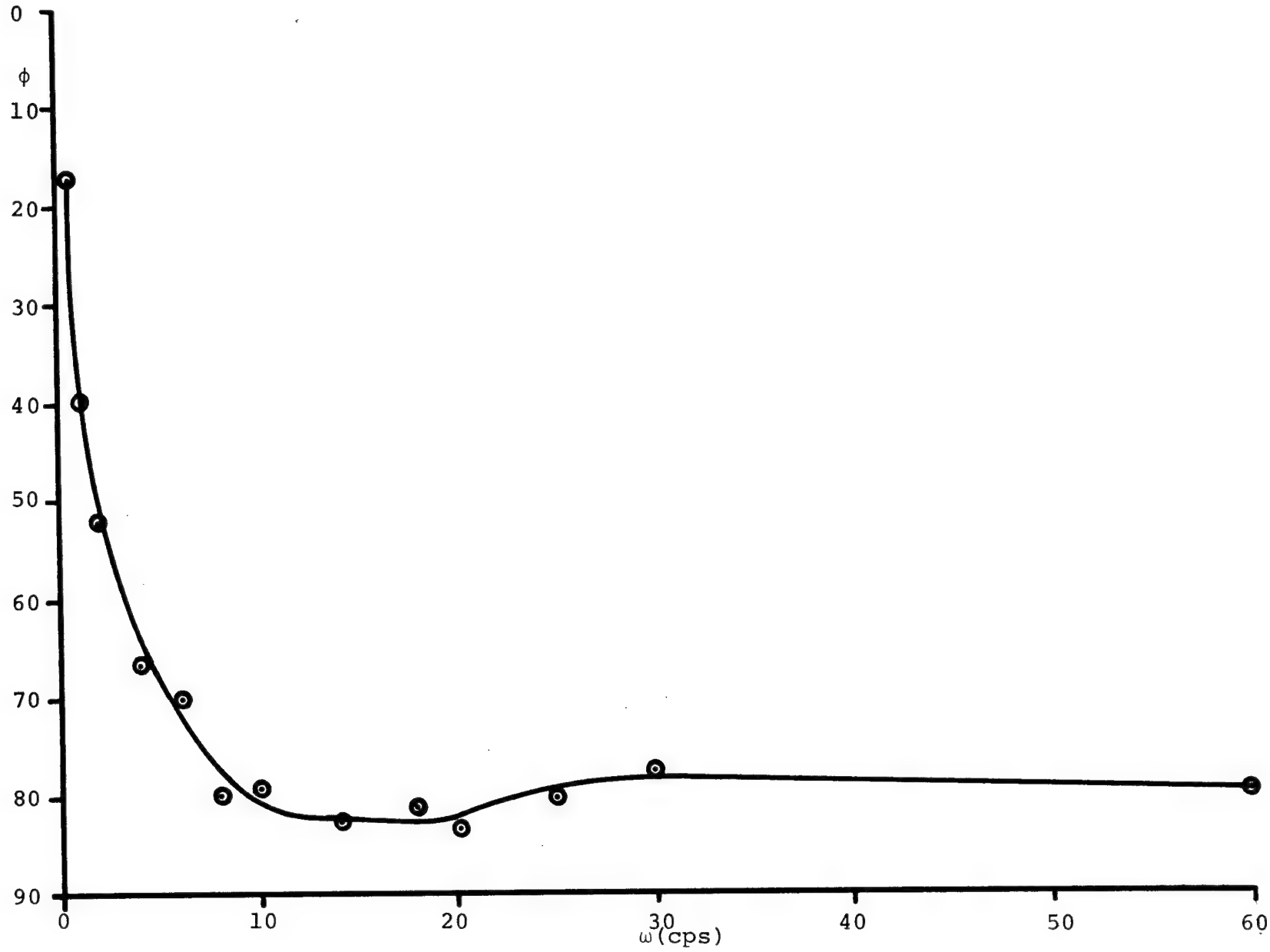

Figure 21 Phase Angle for E_F = 5.0 Volts

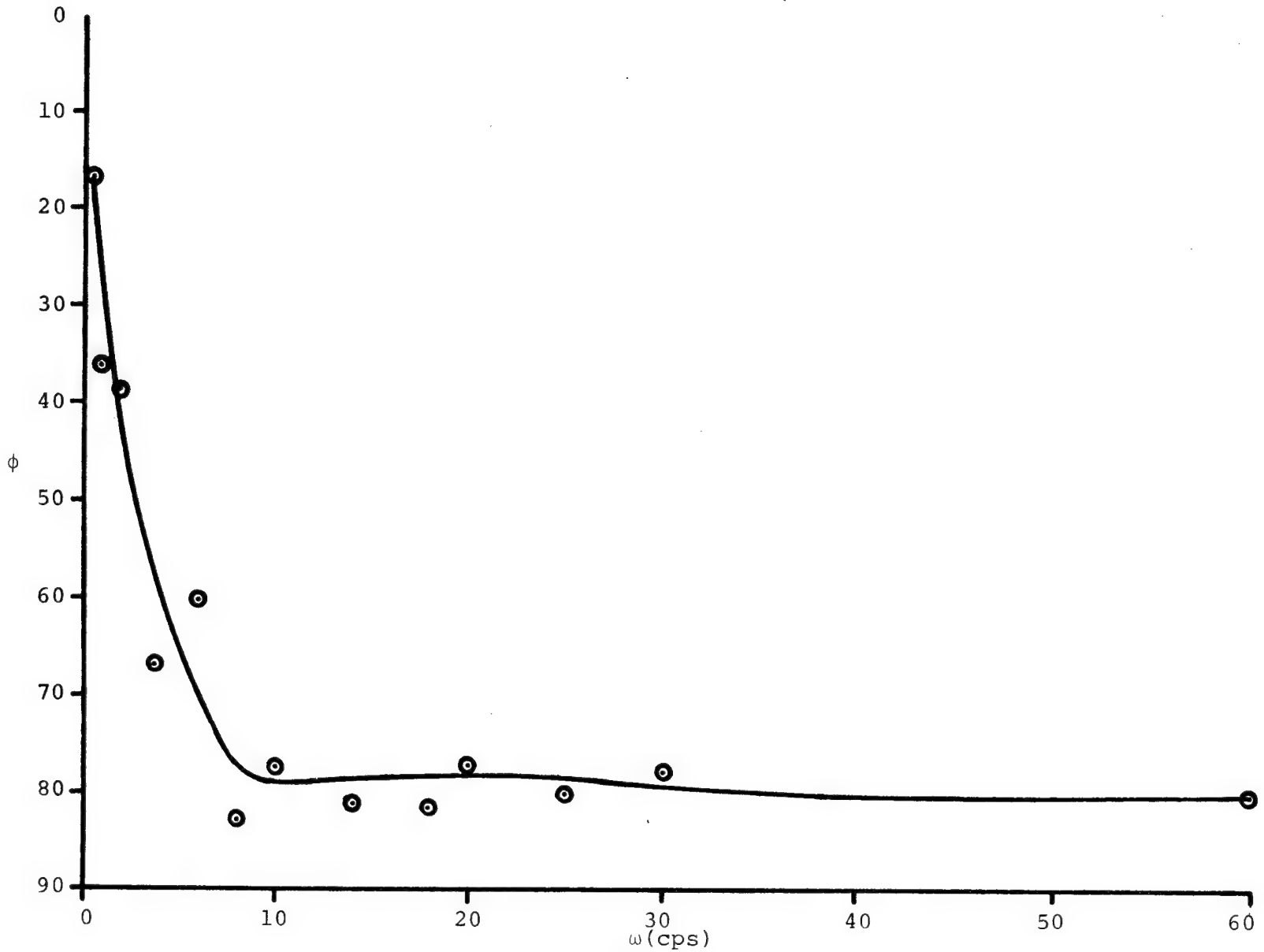

Figure 22 Phase Angle for E_F = 20.0 Volts

DETAILS OF ELLIPTIC CORE SET IN S-CURVE (ZERO-CONING) STANDARD MODEL

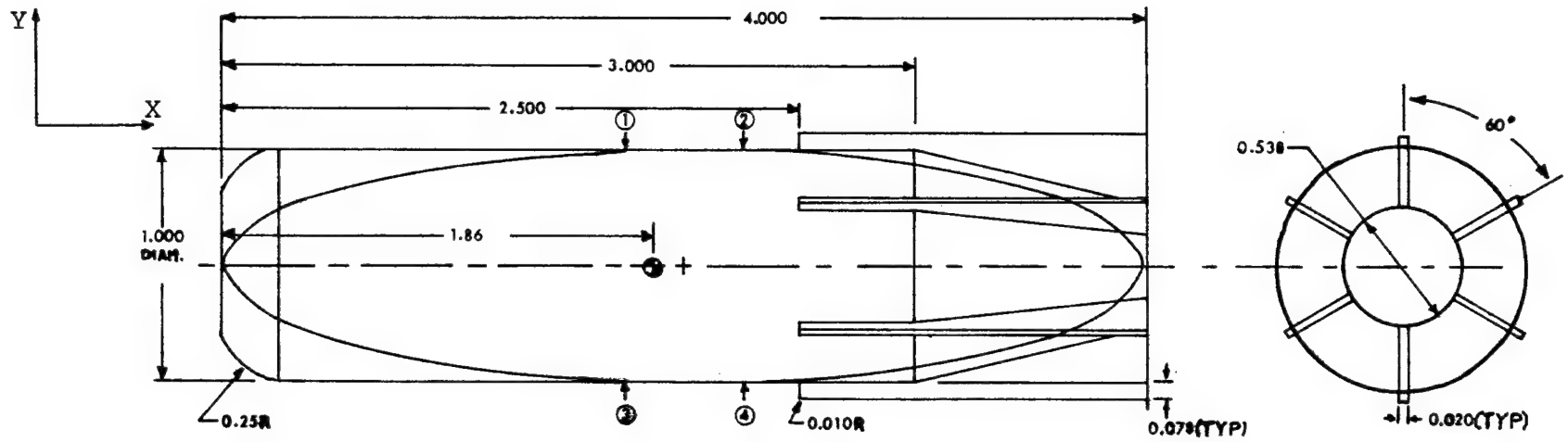

Elliptical Coordinates - see Table 6.

NOTES: 1. All dimensions in inches
2. Solder joints 1, 2, 3 & 4

Figure 23

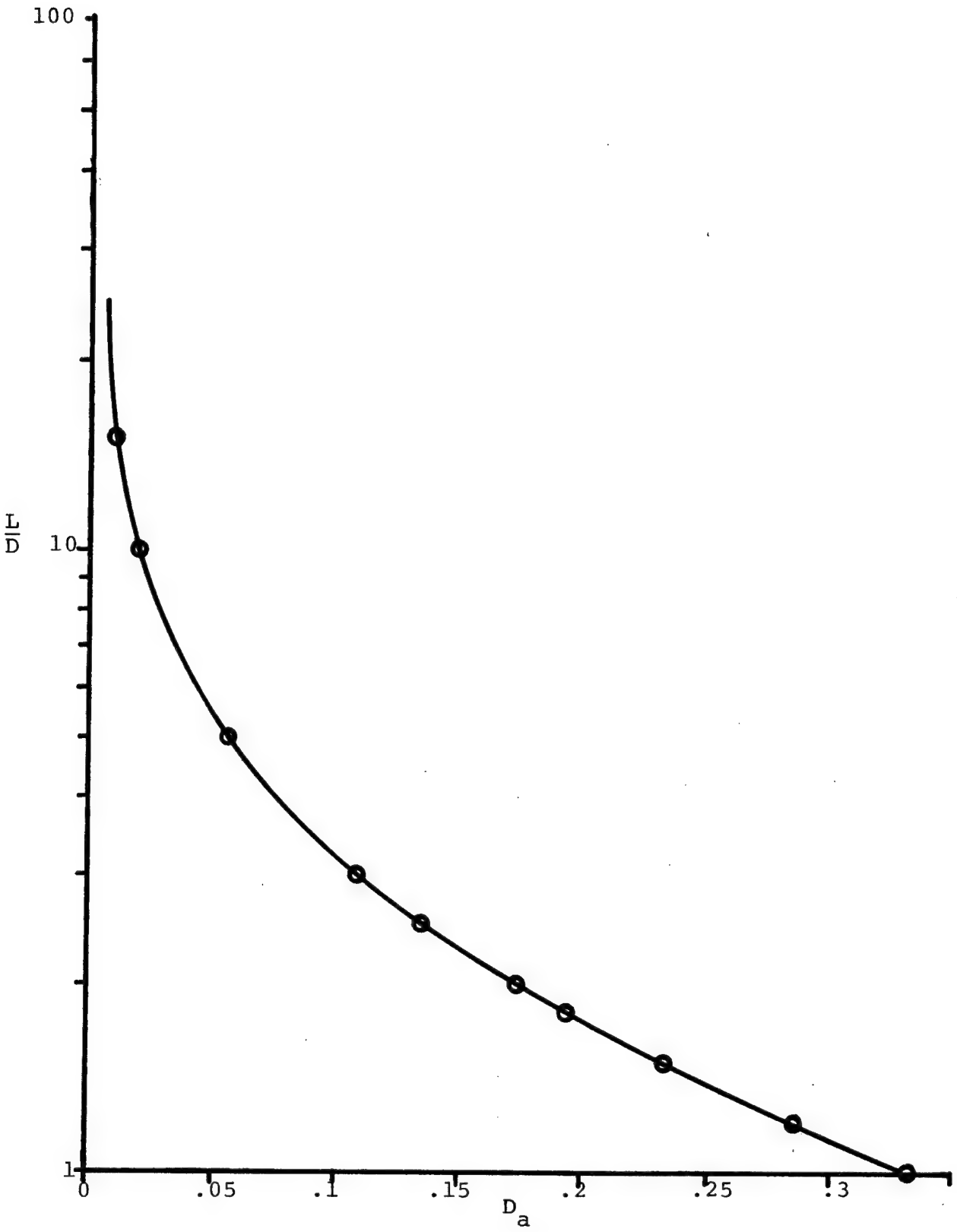

Figure 24 Demagnetizing Factor for Ellipsoids $D_b=D_c=\frac{1}{2}(1-D_a)$

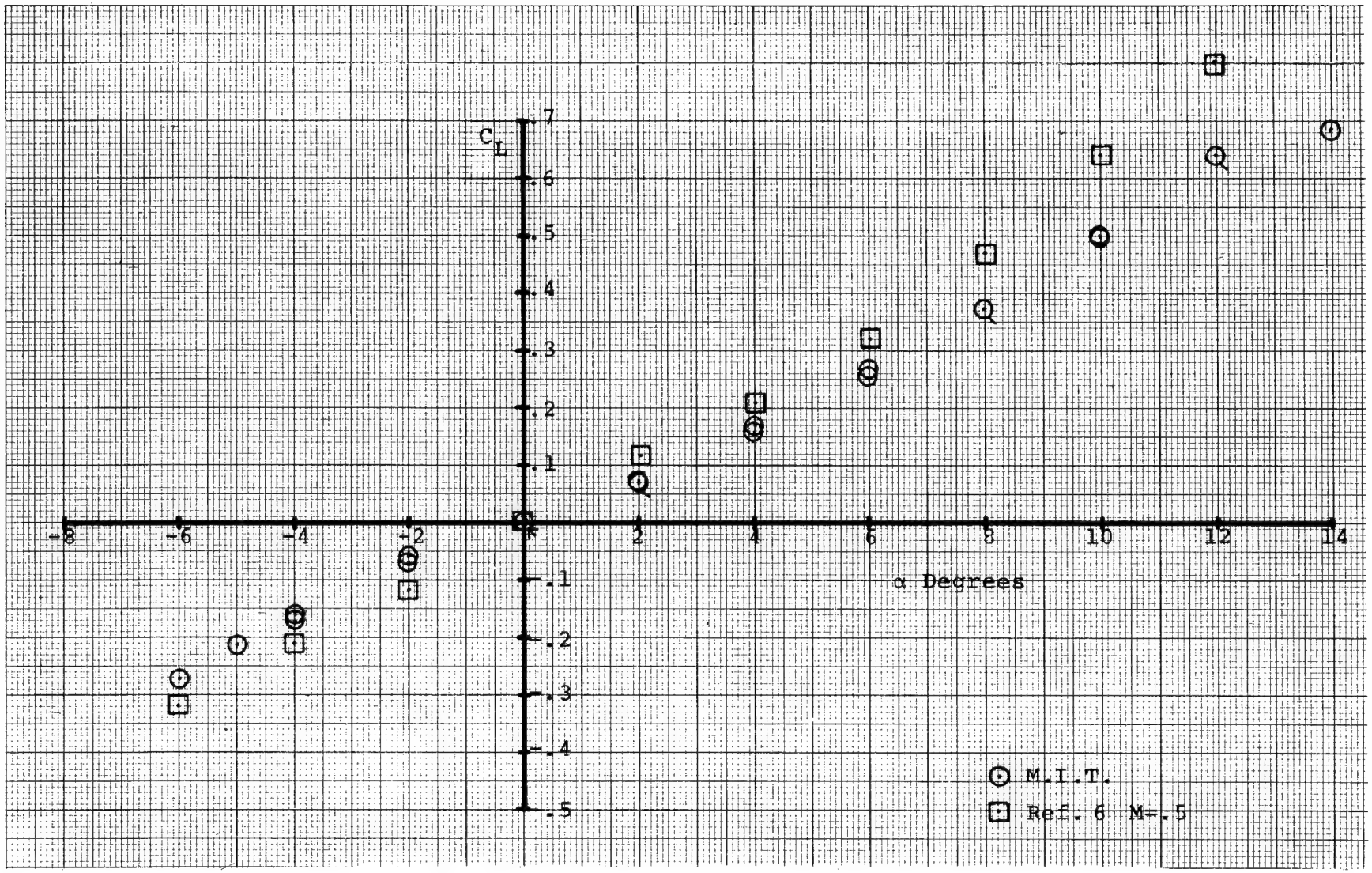

Figure 25 Lift Coefficient versus angle of attack at M=.37, $Re_d=2.1x10^5$

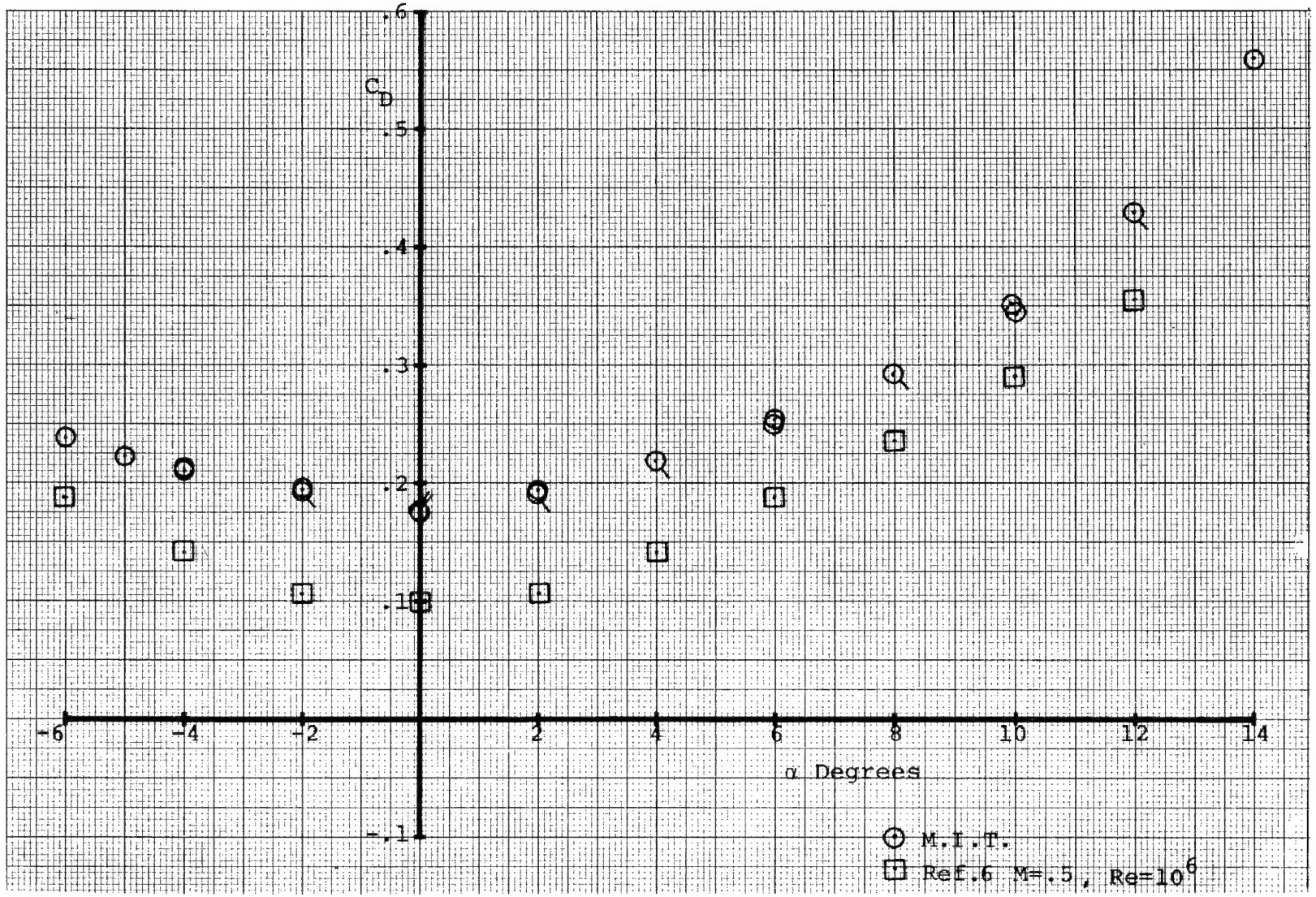

Figure 26 Drag Coefficient versus angle of attack at M=.37, Re_d=2.1x10^5

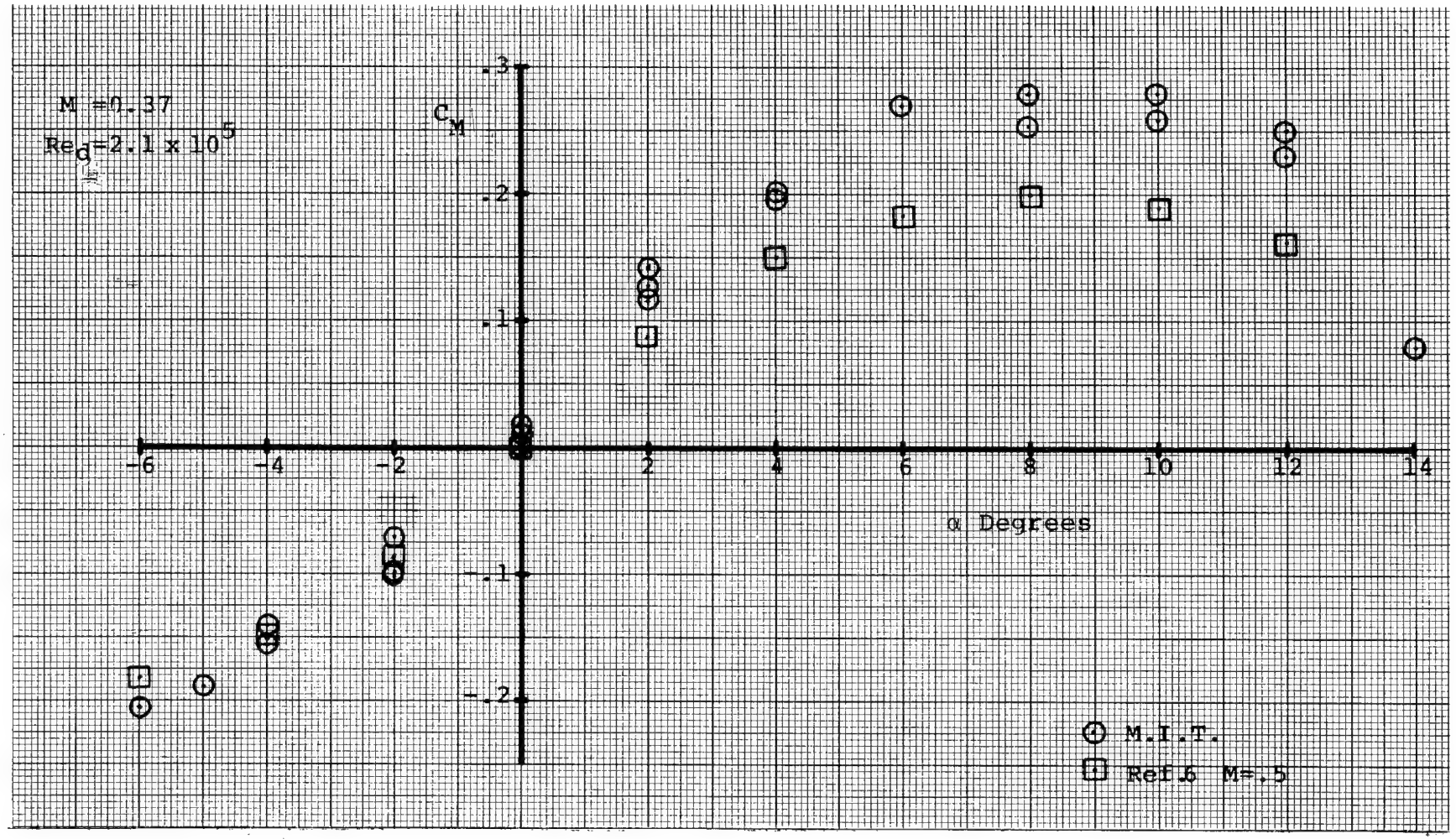

Figure 27 Pitching Moment Coefficient versus angle of attack at M=.37, Re_d=2.1x10^5

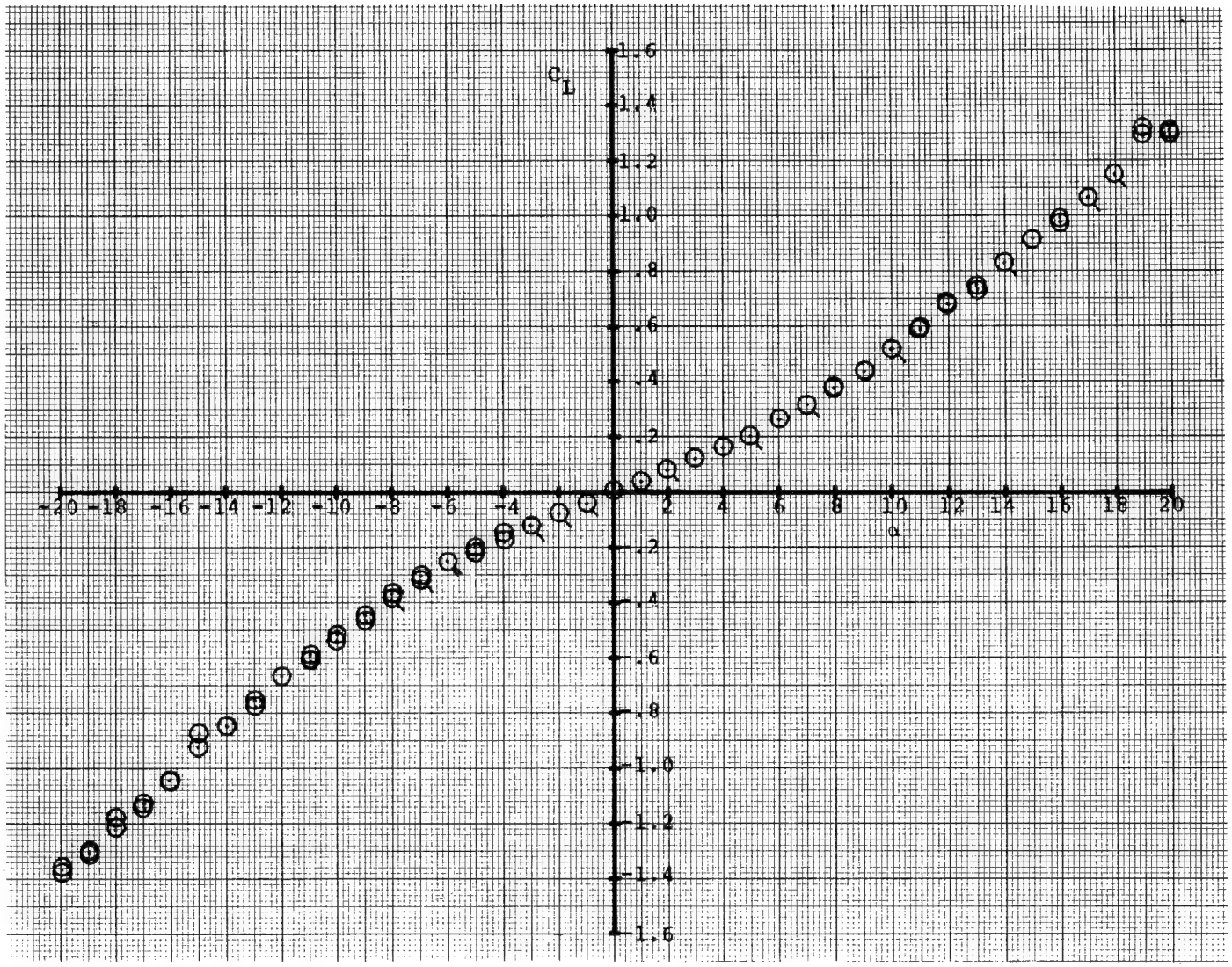

Figure 28 Lift Coefficient versus angle of attack at M=.18, Re_d=1x10^5

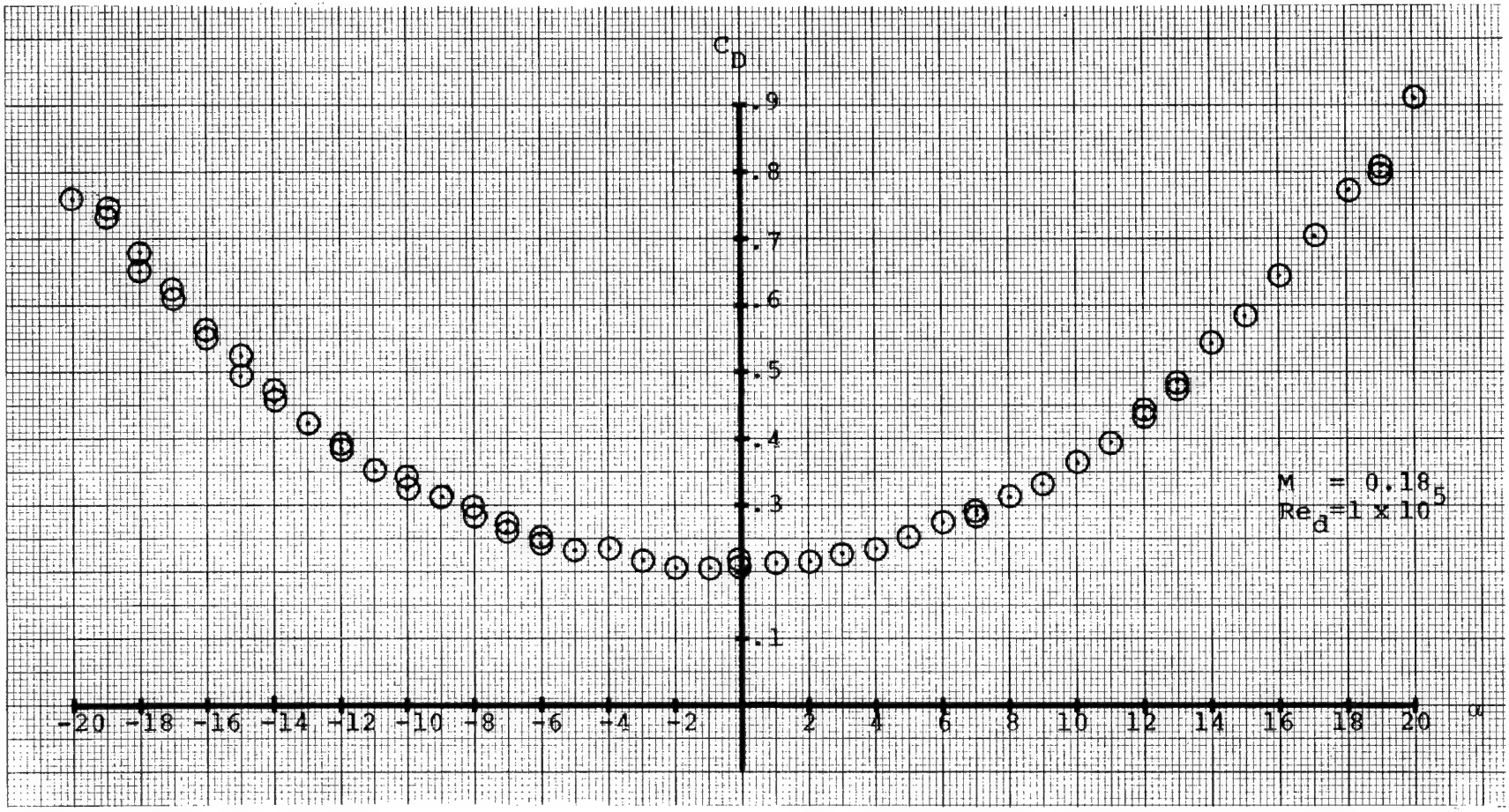

Figure 29 Drag Coefficient versus angle of attack at M=.18, Re_d=1x10^5

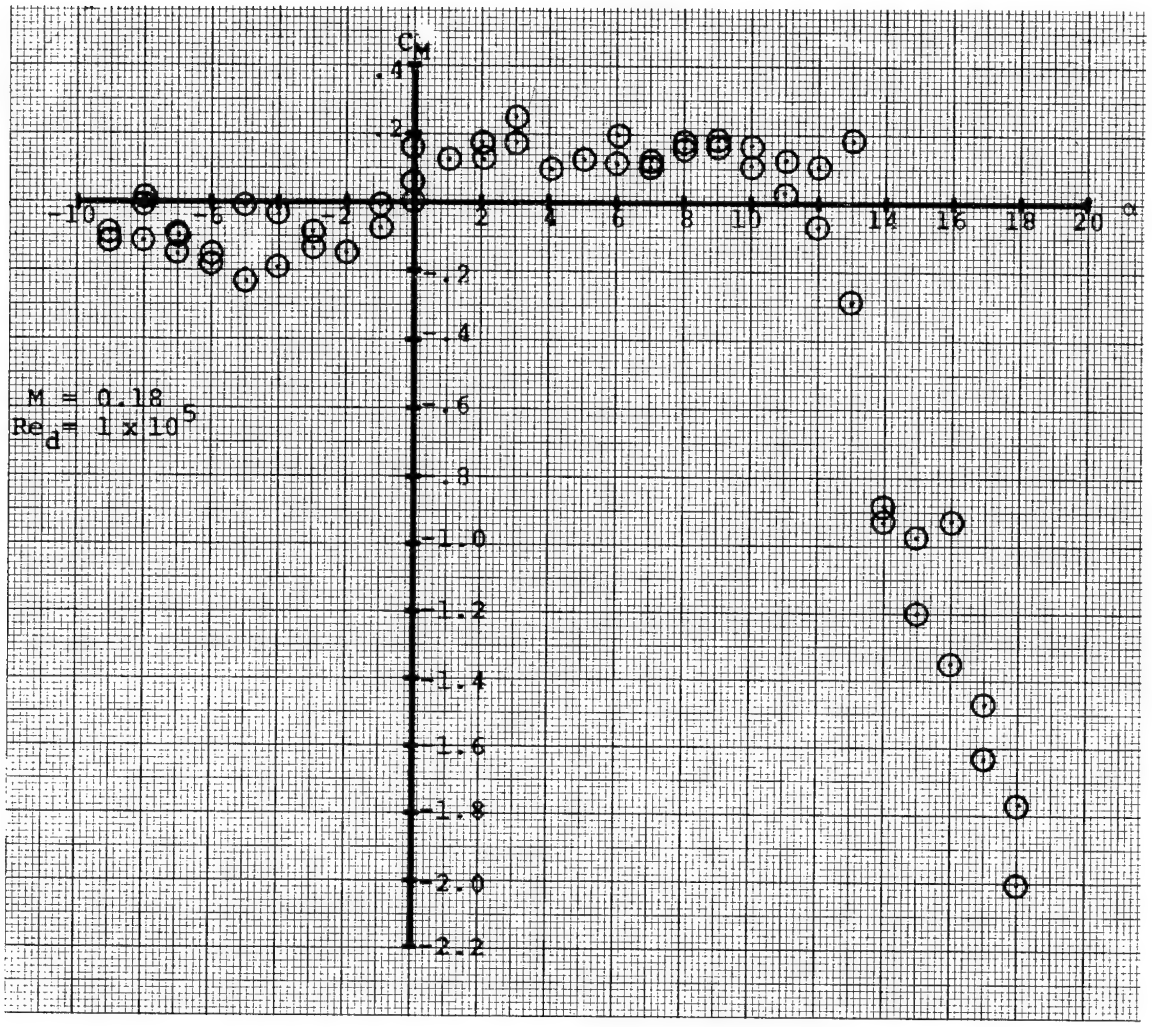

Figure 30 Pitching Moment Coefficient versus angle of attack at M=.18, Re_d=1x10^5, reference 2 calibers from nose.

DISTRIBUTION LIST

	No. Copies
Commander Picatinny Arsenal ATTN: Scientific and Technical Information Branch Dover, NJ 07801	5
Department of the Army Office, Chief of Research and Development Washington, DC 20310	1
Department of the Army Office, Asst Chief of Staff for Force Development Washington, DC 20310	1
Deputy Assistant Secretary of the Army (R&D) ATTN: Mr. C. L. Poor Washington, DC 20310	1
Commander US Army Materiel Command ATTN: AMCRD-RS-PE-BAL, Mr. J. Hughes AMCRD-WN, Mr. W. J. Ralph AMCRD-MT, Mr. E. Sedlack Research and Development Directorate 5001 Eisenhower Avenue Alexandria, VA 22304	3
Commander USA Armament Command ATTN: AMSAR-RDR-Dr. E. Haug AMSAR-RD, Mr. J. A. Brinkman AMSAR-RD, Mr. J. Turkeltaub Rock Island, IL 61201	3
Commander US Army Missile Command ATTN: AMSMI-RFSK, Mr. R. Deep Mr. R. E. Becht AMSMI-RDP AMSMI-RBLD AMSMI-RF Redstone Arsenal, AL 35809	5

	No. Copies
Commander USA Training & Doctrine Command ATTN: ATSF-CF Ft. Monroe, VA 23651	1
Redstone Scientific Information Center US Army Missile Command ATTN: Chief, Document Section Redstone Arsenal, AL 35809	1
Commander USA Field Artillery School ATTN: ATSF-CTD-WR Ft. Sill, OK 73503	1
Commander Ballistic Research Laboratories ATTN: AMXRD-EBL Dr. C. Murphy Mr. R. H. Krieger Mr. L. MacAllister Mr. R. McCoy Mr. A. Platou Aberdeen Proving Ground, MD 21005	5
Commander US Army Frankford Arsenal ATTN: SARFA-MDP, Mr. S. Hirshman Philadelphia, PA 19137	1
Commander US Army Edgewood Arsenal ATTN: Technical Library Edgewood Arsenal, MD 21010	1
Director US Army Advanced Materiel Concepts Agency 2461 Eisenhower Avenue Alexandria, VA 22314	1
Director Advanced Research Projects Agency Department of Defense Washington, DC 20301	1

	No. Copies
PM Cannon Artillery Weapons System ATTN: AMCPM-CAWS, Mr. F. Grossman AMCMP-CAWS-TM, Mr. H. Noble Rock Island, IL 61201	2
PM Selected Ammunition USA Materiel Command ATTN: AMCPM-SA-, Mr. B. Karin Mr. M. Chase Mr. R. Bird Picatinny Arsenal, Dover, NJ 07801	3
PM Lance Millile System USA Materiel Command ATTN: AMCPM-LCE, Mr. L. Seggel Redstone Arsenal, AL 35809	1
Commander Harry Diamond Laboratories ATTN: Library Connecticut Ave & VanNess Streets, NW Washington, DC 20438	1
Chief, Bureau of Naval Weapons Department of the Navy ATTN: IDS-33 Washington, DC 20360	1
Commander & Director Naval Ship Research & Development Center ATTN: Aerodynamics Laboratory Washington, DC 20007	1
Commander US Naval Weapons Center ATTN: Technical Library Dr. W. Haseltine China Lake, CA 93527	2
Commander Naval Ordnance Laboratory ATTN: Research Library Mr. F. Regan Mr. S. Hastings White Oak, Silver Spring, MD 20915	3

	No. Copies
Commander US Naval Weapons Laboratory ATTN: Technical Laboratory Mr. W. Chadwick Mr. C. Wingo Dr. T. Clare Dr. W. Kemper Dahlgren, VA 22448	5
Commander US Naval Ordnance Station ATTN: Mr. D. Monetta Indian Head, MD 20640	1
Director US Army Air Mobility Research & Dev Laboratory Ames Research Center Moffett Field, CA 94035	1
Director NASA Ames Research Center ATTN: Mr. S. Treon Moffett Field, CA 94035	1
Commander Air Proving Ground Center (PGTRI) ATTN: Technical Library Mr. C. Butler Eglin Air Force Base, FL 32542	3
General Electric Company Armament Department ATTN: Mr. R. H. Whyte Room 1412 Lakeside Avenue Burlington, VT 05401	1
Sandia Laboratories ATTN: Aerodynamics Dept. Mr. R. Maydew Mr. W. Curry P.O. Box 5800 Albuquerque, NM 87115	3

	No. Copies
Defense Documentation Center Cameron Station Alexandria, VA 22314	1
Commander Picatinny Arsenal ATTN: Dr. E. G. Sharkoff Mr. J. W. Gregorits Mr. A. A. Loeb Mr. D. H. Mertz Mr. A. King Mr. T. Stevens Mr. R. Smith Mr. S. Wasserman Mr. J. Dubin Mr. J. Matt Mr. R. Kline Mr. C. Cavanaugh Dover, NJ 07801	29